

CHEM MED CHEM

CHEMISTRY ENABLING DRUG DISCOVERY

Accepted Article

Title: Novel, dual target-directed annelated xanthine derivatives acting on adenosine receptors and monoamine oxidase B

Authors: Kamil J Kuder, Michał Załuski, Jakub Schabikowski, Gniewomir Latacz, Agnieszka Olejarz-Maciej, Piotr Jaśko, Andreas Brockmann, Christa E. Müller, and Katarzyna Kieć-Kononowicz

This manuscript has been accepted after peer review and appears as an Accepted Article online prior to editing, proofing, and formal publication of the final Version of Record (VoR). This work is currently citable by using the Digital Object Identifier (DOI) given below. The VoR will be published online in Early View as soon as possible and may be different to this Accepted Article as a result of editing. Readers should obtain the VoR from the journal website shown below when it is published to ensure accuracy of information. The authors are responsible for the content of this Accepted Article.

To be cited as: *ChemMedChem* 10.1002/cmdc.201900717

Link to VoR: <http://dx.doi.org/10.1002/cmdc.201900717>

WILEY-VCH

www.chemmedchem.org

A Journal of



Novel, dual target-directed annelated xanthine derivatives acting on adenosine receptors and monoamine oxidase B

Kamil J. Kuder ^{[a]*‡}, Michał Załuski ^{[a]‡}, Jakub Schabikowski ^[a], Gniewomir Latacz ^[a], Agnieszka Olejarz-Maciej ^[a], Piotr Jaśko ^[a], Agata Doroz-Płonka ^[a], Andreas Brockmann ^[b], Christa E. Müller ^[b], Katarzyna Kieć-Kononowicz ^[a]

[a] *Dr. Kamil J. Kuder; Michał Załuski; Jakub Schabikowski; Dr. Gniewomir Latacz; Agnieszka-Olejarz Maciej; Agata Doroz-Płonka; Piotr Jaśko; Prof. Katarzyna Kieć-Kononowicz
Department of Technology and Biotechnology of Drugs
Jagiellonian University Medical College, Faculty of Pharmacy
Medyczna 9, 30-688 Kraków, Poland
E-mail: kamil.kuder@uj.edu.pl

[b] Andreas Brockman, Prof. Christa Müller
PharmaCenter Bonn, Pharmaceutical Institute
Pharmaceutical Chemistry University of Bonn
An der Immenburg 4, 53121 Bonn, Germany

‡ these authors contributed equally

Supporting information for this article is given via a link at the end of the document

Abstract: Annelated purinedione derivatives have been shown to act as possible multiple target ligands, addressing adenosine receptors and monoaminooxidases. Within this study, based on our previous results, novel annelated pyrimido- and diazepino[2,1-f]purinedione derivatives were designed as dual-target-directed ligands combining A_{2A} adenosine receptor (AR) antagonistic activity with blockade of monoamine oxidase B. A library of 20 novel compounds was synthesized and biologically evaluated in radioligand binding studies at AR subtypes and for their ability to inhibit MAO-B. This allowed for identification of 9-(2-chloro-6-fluorobenzyl)-3-ethyl-1-methyl-6,7,8,9-tetrahydropyrimido[2,1-f]purine-2,4(1*H*,3*H*)-dione (**13e**; K_i human A_{2A}AR: 264 nM and IC₅₀ human MAO-B: 243 nM) as the most potent dual acting ligand from this series. ADMET parameters were estimated in vitro and analysis of structure-activity relationships was complemented by molecular docking studies based on previously published X-ray structures of the protein targets. Such dual acting ligands, by selectively blocking A_{2A} AR, accompanied by the inhibition of dopamine metabolizing enzyme MAO-B might provide symptomatic and neuroprotective effects in, among others, Parkinson disease treatment

Introduction

Nowadays, as stated by the WHO ^[1], most people can expect to live even beyond their 60's. However, this trend has significant impact on the structure of the human population which is ageing. As a result of this process, an increase in the occurrence of neurodegenerative diseases (ND) such as e.g. Parkinson's (PD) and Alzheimer's (AD) are observed. The progress of these diseases is gradual and irreversible, leading to the degeneration of neurons, and to inflammatory processes in the brain. So far, treatment strategies for NDs are sparse due to the lack of full knowledge of their complex pathogenesis. Drugs that interact with only one protein target might not fully reverse or retard the

ongoing destructive process in NDs and prevent them from progression ^[2,3]. Thus, in contrast to the classical, "one target - one drug" paradigm, a multi-target-directed ligand (MTDL) strategy may be superior ^[4,5]. MTDLs through their synergistic mechanism of action might exhibit high therapeutic efficacy and increase patients' compliance, and show a reduced risk of side effects due to drug-drug interactions ^[6-9]. One of the proposed multi-target strategy is the combination of adenosine A_{2A} receptors (A_{2A}ARs) blockade with inhibition of monoamine oxidase B (MAO-B) ^[10-12]. This combination has been described to not only providing symptomatic relief, but also display neuroprotective activity.

The use of A_{2A}AR antagonists in PD treatment is supported by several findings: A_{2A}ARs co-localize with dopamine D₂ receptors in the striatum, and their inhibition enhances D₂-dependent signaling; A_{2A}AR antagonists reduce production of cAMP by inhibiting A_{2A}AR activation of cyclic adenylylase ^[13-15]. Moreover A_{2A}AR antagonists might reduce the formation of β-amyloid plaque ^[16,17] and were shown to induce neuroprotective effects in several studies ^[18-21].

MAO-B inhibitors are widely used therapeutics in PD, often combined with levodopa, mostly in early stages of disease, when the dopamine levels are not severely compromised yet. Apart from dopamine metabolism, they also inhibit the formation of H₂O₂ by MAO-B activity ^{[7][22,23]}. However, selectivity over MAO-A isoform is desired to avoid a potential hypertensive crisis ^[24].

One of the most widely used natural central stimulants, caffeine (**1**), although being a weakly potent AR antagonist and non-selective for AR subtypes, has been proven beneficial in PD and AD treatment ^[21,25,26]. Its xanthine core serves as a versatile scaffold. Substitution in position 8 with styryl substituents led to the discovery of the potent A_{2A} AR antagonists istradefylline (**2a**) and CSC (8-chlorostyrylcaffeine **2b**, Figure 1). While the first one was approved in Japan for adjunct PD therapy, and recently also in the USA, CSC is the first A_{2A} AR with ancillary MAO-B inhibitory activity ^[27,28].

FULL PAPER

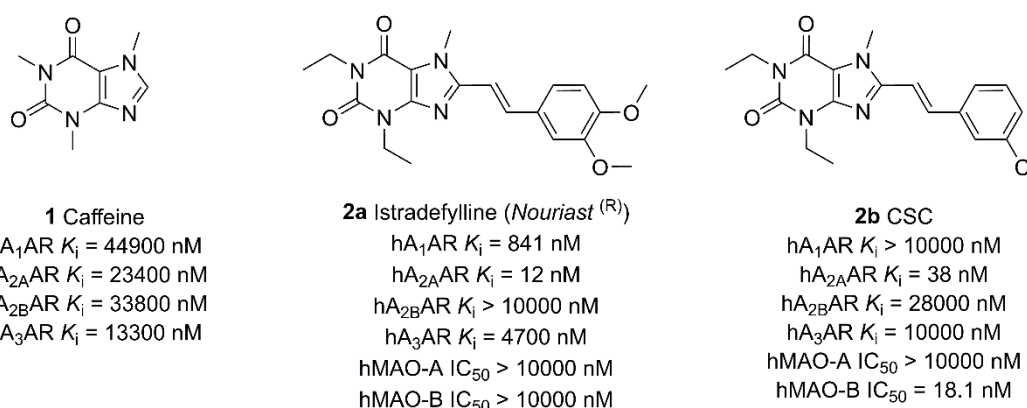


Figure 1 Structures and affinities for selected targets of potent xanthine derivatives

Recent studies from our groups led to the identification of tricyclic pyrimido[2,1-*f*]purinedione and diazepino[2,1-*f*]purinedione derivatives as bioisosters of (*E*)-8-styrylxanthine. Exchange of the 2-methoxybenzyl substituent of compound **3a** [29] by a lipophilic 2-fluoro-6-chlorobenzyl moiety in compound **3b** resulted in an increase in MAO-B inhibitory potency (Figure 2). Moreover, reduction of N3 substituent to methyl resulted in higher A_{2A} AR selectivity. On the other hand, enlargement of the annelated ring (**4**) led to a decline in AR affinity, but at the same time, an increase in MAO-B inhibitory activity was observed [30].

On the basis of the abovementioned findings we designed a new series of expected dual target ligands, A_{2A} antagonists/MAO-B inhibitors. Structures were based on the 1,3-dimethylxanthine

scaffold with an annelated pyrimidine or diazepine ring fused to the *f*-bond, using various alkyl substituents in the N1- and N3-position and substituted benzyl moieties in position N9 (N10 for diazepine derivatives, Figure 3). Through such variations, we wanted to test their influence on activity and selectivity for the investigated targets. Furthermore, the impact of the fused heterocyclic ring size on inhibition of MAO-B and affinity for A_{2A} ARs was evaluated. To rationalize the observed biological activities, molecular docking studies using the available human AR and MAO-B crystal structures were performed for the new compounds. Moreover, selected molecular and ADMET (absorption, distribution, metabolism, excretion, toxicity) properties were tested *in vitro*.

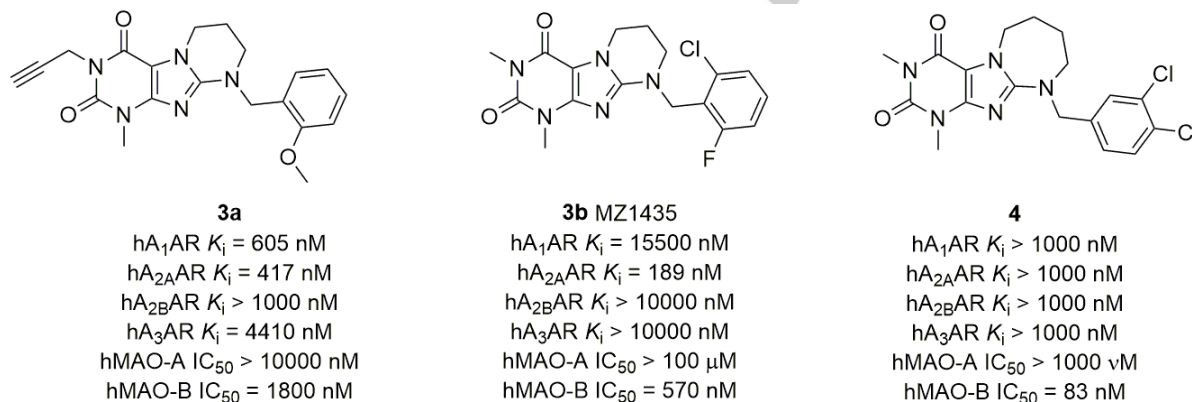


Figure 2 Structures and affinities of previously obtained potent compounds from our groups

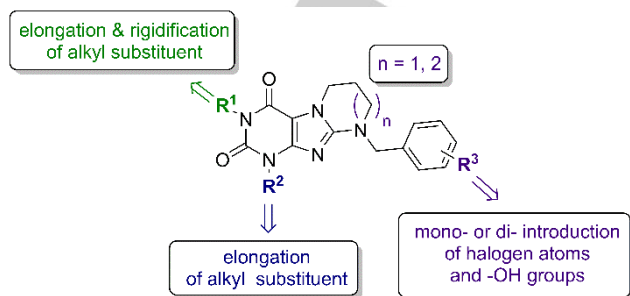


Figure 3 General structure of herein described ligands, and proposed lead structure modifications

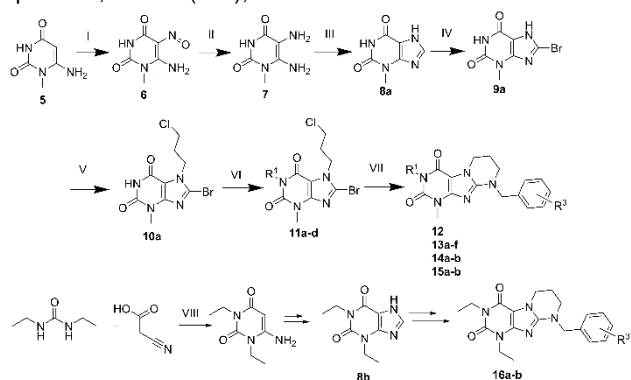
Results and Discussion

Chemistry

Synthesis of tricyclic pyrimido[2,1-*f*]purinediones **12-16** with an aromatic residue in the 9-position of the annelated xanthine was performed by a seven-step procedure as shown in Scheme 1. 6-Amino-1-methylpyrimidine-2,4(1*H*,3*H*)-dione (**5**) was transformed into 3-methylxanthine (**8a**) by nitrosation, reduction with sodium hydrosulfite and ring closure. Subsequent bromination according to a previously described method [31] yielded 8-bromo-3-methyl-

FULL PAPER

3,7-dihydro-1*H*-purine-2,6-dione (**9a**). N7-alkylation in dimethylformamide with 1-bromo-3-chloropropane and DIPEA providing 8-bromo-7-(3-chloropropyl)-3-methyl-3,7-dihydro-1*H*-purine-2,6-dione (**10a**), which was further substituted in the N1-

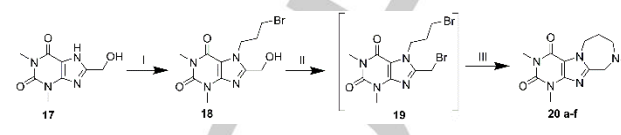


Scheme 1 Synthetic routes for described pyrimido [2,1-*f*] purinediones; I – NaNO₂, H⁺; II – Na₂S₂O₄; III – HCOOH; NaOH; IV – HBr, NaClO₃; V – 1-Br-3-Cl-propane, DIPEA, DMF; VI- Br-ethane /propane /propargyl, K₂CO₃; VII – substituted benzylamine, (Et)₃N, propanol, sealed tube, microwave irradiation; VIII - (CH₃CO)₂O; AcOH, 70 °C. Detailed description can be found in Experimental section.

position with five different alkyl substituents to provide **11a-d**. Diversity was introduced in the last step by different aromatic residues during the ring closure reaction with various benzyl amines.

N1,N3-diethyl derivatives **16a, b** were obtained using a previously described procedure starting from N,N'-diethylurea [31]. Synthesis of tricyclic 1,3-dimethyldiazepino[2,1-*f*] purinediones was performed in a three-step procedure as depicted in Scheme 2. The previously obtained [32] 1,3-dimethyl-8-hydroxymethylxanthine (**17**) was alkylated at the 7-position by reaction with 1,3-dibromopropane in the presence of potassium

carbonate. The hydroxy function of **18** was subsequently converted to the corresponding bromide by treatment with phosphorus tribromide. The resulting 7-(3-bromopropyl)-8-(bromomethyl)-1,3-dimethylpurine-2,4-dione (**19**) was not isolated, but directly reacted with mono- or disubstituted benzylamine. The structures of all products were confirmed by NMR and MS analyses



Scheme 2 Synthetic routes for described diazepino[2,1-*f*]purinediones: I – 1,3-dibromopropane, K₂CO₃, DMF; II – PBr₃, CH₂Cl₂, 0 °C – rt; III – substituted benzylamine, (Et)₃N, propanol, sealed tube, microwave irradiation, 150 °C, 300 W. Detailed description can be found in Experimental section

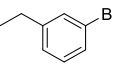
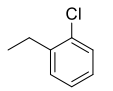
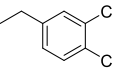
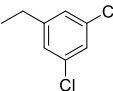
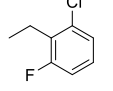
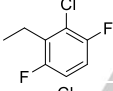
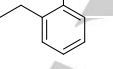
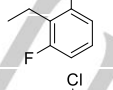
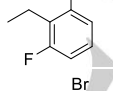
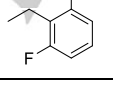
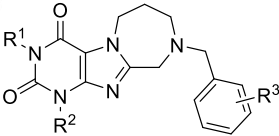
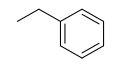
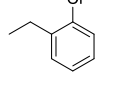
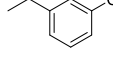
Biological evaluation

In order to evaluate the new compounds' affinity for all four AR subtypes, they were tested in radioligand binding assays at cell membrane preparations. Human adenosine A_{2A} and A_{2B} receptors were recombinantly expressed in HEK293 cells. Human A₁ and A₃ ARs were recombinantly expressed in Chinese hamster ovary (CHO) cells. [³H]2-Chloro-N⁶-cyclopentyladenosine ([³H]CCPA), [³H]3-(3-hydroxypropyl)-1-propargyl-7-methyl-8-(*m*-methoxystyryl)xanthine ([³H]MSX-2), [³H]8-(4-(4-(4-chlorophenyl)piperazine-1-sulfonyl)phenyl)-1-propylxanthine ([³H]PSB-603) and [³H]2-phenyl-8-ethyl-4-methyl-(8*R*)-4,5,7,8-tetrahydro-1*H*-imidazo[2,1-*f*]purine-5-one ([³H]PSB-11) were used as radioligands for A₁, A_{2A}, A_{2B} and A₃AR binding studies, respectively [33–36]. Moreover, all new compounds were tested for their inhibitory potency at human MAO-B, and selected compounds were additionally tested for selectivity versus human MAO-A

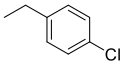
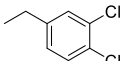
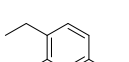
Table 1 Structures and adenosine receptors affinity for the group of described compounds

Compound ^[a]	R ¹	R ²	R ³	A ₁ ADENOSINE RECEPTOR vs. [³ H]CCPA	A _{2A} ADENOSINE RECEPTOR vs. [³ H]MSX-2	A _{2B} ADENOSINE RECEPTOR vs. [³ H]PSB-603	A ₃ ADENOSINE RECEPTOR vs. [³ H]PSB-11
K _i ± SEM [nM] (% Inhibition ± SEM at 1 μM)							
1 (Caffeine)				44 900	23 400	33 800	13 300
2a Istradefylline				841	12	10000	4700
3b	-CH ₃	-CH ₃		15500	189	10000	10000
12 MZ-1470	-CH ₃	-CH ₃		>1000 (-1 ± 3)	>1000 (6 ± 3)	>1000 (3 ± 4)	>1000 (-5 ± 2)

FULL PAPER

Compound ^[a]	R ¹	R ²	R ³	A ₁ ADENOSINE RECEPTOR vs. [³ H]CCPA	A _{2A} ADENOSINE RECEPTOR vs. [³ H]MSX-2	A _{2B} ADENOSINE RECEPTOR vs. [³ H]PSB-603	A ₃ ADENOSINE RECEPTOR vs. [³ H]PSB-11
<i>K_i</i> ± SEM [nM] (% Inhibition ± SEM at 1 μM)							
13a MZ-1521	-C ₂ H ₅	-CH ₃		n.d	2050 ± 214	>1000 (23 ± 3)	>1000 (23 ± 4)
13b MZ-1507	-C ₂ H ₅	-CH ₃		>1000 (20 ± 8)	1390 ± 283	>1000 (25 ± 1)	>1000 (19 ± 7)
13c MZ-1517	-C ₂ H ₅	-CH ₃		>1000 (2 ± 9)	>1000 (32 ± 3)	>1000 (6 ± 1)	>1000 (23 ± 11)
13d MZ-1519	-C ₂ H ₅	-CH ₃		>1000 (42 ± 4)	>1000 (35 ± 8)	>1000 (3 ± 1)	>1000 (32 ± 5)
13e MZ-1504	-C ₂ H ₅	-CH ₃		>1000 (3 ± 13)	264 ± 106 (80 ± 6)	>1000 (16 ± 13)	>1000 (16 ± 7)
13f MZ-1518	-C ₂ H ₅	-CH ₃		n.d.	1550 ± 244	>1000 (12 ± 6)	>1000 (17 ± 0)
14a MZ-1468	-C ₃ H ₇	-CH ₃		>1000 (19 ± 1)	2660 ± 703	>1000 (21 ± 4)	>1000 (29 ± 1)
14b MZ-1501	-C ₃ H ₇	-CH ₃		>1000 (3 ± 9)	504 ± 79 (67 ± 6)	>1000 (33 ± 1)	>1000 (23 ± 8)
15a MZ-1469	-C ₃ H ₃	-CH ₃		>1000 (26 ± 5)	1260 ± 314	>1000 (38 ± 1)	>1000 (22 ± 1)
15b MZ-1502	-C ₃ H ₃	-CH ₃		>1000 (27 ± 4)	207 ± 51 (79 ± 3)	>1000 (32 ± 14)	>1000 (16 ± 3)
16a MZ-1492	-C ₂ H ₅	-C ₂ H ₅		>1000 (34 ± 14)	238 ± 38 (88 ± 8)	>1000 (27 ± 6)	>1000 (19 ± 3)
16b MZ-1500	-C ₂ H ₅	-C ₂ H ₅		>1000 (28 ± 7)	240 ± 90 (81 ± 6)	>1000 (26 ± 13)	>1000 (19 ± 3)
							
20a JS-17001	-CH ₃	-CH ₃		>1000 (7 ± 3)	>1000 (33 ± 16)	>1000 (24 ± 7)	>1000 (5 ± 10)
20b JS-17002	-CH ₃	-CH ₃		>1000 (23 ± 3)	>1000 (6 ± 3)	>1000 (0 ± 3)	>1000 (6 ± 8 / 1 μM)
20c JS-17003	-CH ₃	-CH ₃		>1000 (16 ± 1)	>1000 (24 ± 18)	>1000 (15 ± 10)	>1000 (-1 ± 3)

FULL PAPER

Compound ^[a]	R ¹	R ²	R ³	A ₁	A _{2A}	A _{2B}	A ₃
				ADENOSINE RECEPTOR vs. [³ H]CCPA	ADENOSINE RECEPTOR vs. [³ H]MSX-2	ADENOSINE RECEPTOR vs. [³ H]PSB-603	ADENOSINE RECEPTOR vs. [³ H]PSB-11
				K _i ± SEM [nM] (% Inhibition ± SEM at 1 μM)			
				At 0,1 μM			
20d JS-17004	-CH ₃	-CH ₃		>1000 (-4 ± 3)	>1000 (12 ± 1)	>1000 (12 ± 1)	>1000 (-1 ± 5)
20e JS-17005	-CH ₃	-CH ₃		>1000 (37 ± 5)	>1000 (26 ± 7)	>1000 (14 ± 5)	>1000 (10 ± 5)
20f JS-17006	-CH ₃	-CH ₃		>1000 (25 ± 5)	>1000 (9 ± 3) at 0,1 μM	>1000 (16 ± 0)	>1000 (7 ± 1)

Structure-activity relationships

Adenosine receptors

The herein presented structures can be divided in two groups according to the size of annelated rings: N9-substituted 1,3-dialkylpyrimido[2,1-*f*]purinediones (**12-16b**) and N10-substituted 1,3-dimethyldiazepino[2,1-*f*]purinediones (**20a-f**). Structural information along with adenosine receptors affinities of the compounds are collected in Table 1, and the pictorial representation of SAR can be found on Figure 4.

None of the tested compounds showed affinity towards A₁, A_{2B}, or A₃ receptors at the highest tested concentration. Among various substituted aromatic groups at N9 or N10 (for pyrimido and diazepino derivatives, respectively) only 2-bromobenzyl (**15a**) and 2-chloro-6-fluorobenzyl moieties (**13e**, **14b**, **15b**, **16b**) appeared to positively influence affinity towards the A_{2A} AR at comparable levels. Introduction of the other, mostly mono-, or dichloro-substituted derivatives resulted in compounds devoid of affinity, which is in agreement with our previous findings^[30]. While paying attention to the N1- and N3-substituents, for the set of active compounds it can be observed, that the elongation of the N3-methyl substituent of compound **3b** to ethyl, or propyl resulted in a slight reduction in affinity, e.g.: compd. **13e** vs. **14b** (hA_{2A}AR K_i = 189 nM and 264 nM vs. 504 nM, respectively). However, rigidification of the propyl group to propargyl resulted in the most potent A_{2A}AR ligand of this group, **15b** (A_{2A}AR K_i = 207 nM). Exchange of the N1-methyl group for ethyl appeared to be tolerated with slight effect on the A_{2A} AR affinity, see **13e** vs. **16b**. In case of [1,4]diazepino[2,1-*f*]purinedione derivatives **20a-f**, the shift of the nitrogen atom from position 10 to 9 in comparison with

recently described [1,3]diazepino[2,1-*f*]purinedione derivatives^[30] resulted in a decline of AR affinity, independently of the introduced aromatic substituent.

MAO-B

All of the herein presented compounds were tested for their inhibitory activity toward MAO-B. For the most promising compounds selectivity toward MAO-A was also evaluated. Test results are collected in Table 2.

Among the 1,3-dialkylpyrimido[2,1-*f*]purinediones, all of the 1-methyl-3-ethyl derivatives (**13a-13f**) showed MAO-B inhibition at nanomolar concentrations, regardless of various eastern molecule part moieties, with most active being dichlorobenzyl derivative **13c** (MAO-B IC₅₀ = 89 ± 0.275 nM). In fact, extension of the N3-substituent by one methylene group (**13e**) resulted in an increased inhibitory potency, as compared with N1,N3-dimethyl analogue **3b** (MAO-B IC₅₀ = , 243 nM and 570 nM respectively). Further elongation of the N3-substituent to propyl resulted in a decrease in inhibitory activity, e.g. compound **14a** vs. **13b**. Unlike observed for AR affinity, rigidification of the propyl chain to a propargyl moiety resulted in reduced MAO-B inhibitory activity (**14a** vs. **15a**). However, exchange of the N1,N3-dimethyl substituents in **3b** for N1,N3-diethyl resulted in a decline in inhibitory potency of homologue **16b**.

Again the shift of the nitrogen atom from position 10 to 9 (**20a-f**) in comparison with recently described [1,3]diazepino[2,1-*f*]purinedione derivatives^[30] resulted in a decline in activity also at MAO-B.

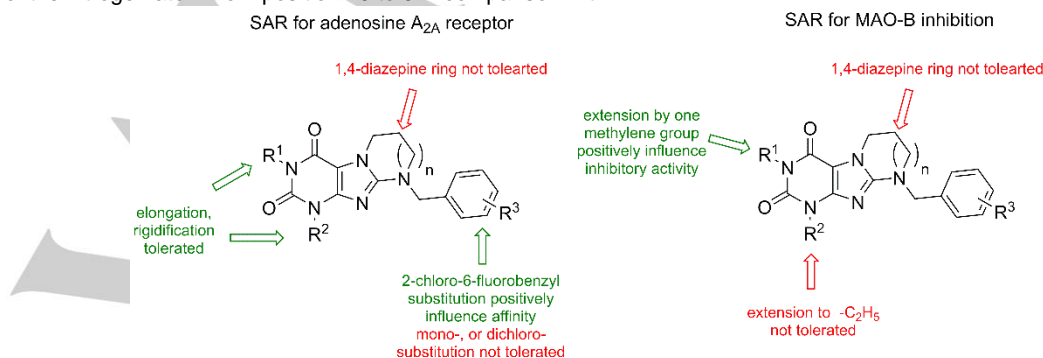


Figure 4 Pictorial representation of SAR for both tested targets

FULL PAPER

Table 2 MAO-A and MAO-B inhibitory activity of tricyclic xanthine derivatives; nd - not determined

Compound	MAO-A	MAO-B ¹
	IC ₅₀ ± SEM (% inhibition at 100 μm)	IC ₅₀ ± SEM (nM) (% inhibition at 1 μm)
21Rasagiline	nd	15400 (100%)
2b CSC	>10000	18.01
4	>1000	83
12 MZ-1470	nd	(48%)
13a MZ-1521	(11%)	212 ± 5.30
13b MZ-1507	23	213 ± 43
13c MZ-1517	nd	89 ± 0.275
13d MZ-1519	nd	306 ± 0.65
13e MZ-1504	(34%)	242.67 ± 45.32 (87%)
13f MZ-1518	nd	143 ± 2.45
14a MZ-1468	(22%)	497.53 ± 80.81 (80%)
14b MZ-1501	nd	1228.2 ± 131.61 (64%)
15a MZ-1469	nd	824.07 ± 195.05 (68%)
15b MZ-1502	nd	1241 ± 36 (53%)
16a MZ-1492	nd	1460 ± 222
16b MZ-1500	nd	(36%)
20a JS-17001	nd	(6%)
20b JS-17002	nd	(8%)
20c JS-17003	nd	(7%)
20d JS-17004	nd	(8%)
20e JS-17005	nd	(14%)
20f JS-17006	nd	(10%)

ADMET estimation *in vitro*

ADMET parameters were estimated *in vitro* for the dual acting 2-chloro-6-fluorobenzyl derivative **13e** and 2-bromobenzyl derivative **16a** according to previously described assay protocols [37–40].

The potential risk of drug-drug interactions (DDI) was first examined by luminescence-based CYP3A4P450-Glo™, CYP2D6P450-Glo™, CYP2C9P450-Glo™ assays and Pgp-Glo™ assays provided by Promega®. The results from Pgp assays showed that both xanthine derivatives are strong substrates of P-glycoprotein (Pgp). The luminescently detected ATP consumption by Pgp increased significantly in the presence of **13e** and **16a** (100 μM) even more than for the reference Pgp substrate verapamil (VPL, 200 μM). No statistically significant increase in ATP consumption for the Pgp-negative xanthine derivative caffeine^[41] was observed (Figure 5A). Moreover, **13e** and **16a** inhibited at 10 μM the activity of the CYP isoforms CYP3A4, 2D6 and 2C9 (Figure 5B, C and D), which are most important in drug metabolism. The strongest inhibition potential (more than 50%) showed **13e** and **16a** for CYP2C9 (Figure 5D) and **16a** for CYP3A4 (Figure 5B). Taking into account the aforementioned results a high DDI potential for **13e** and **16a** has to be considered. Moreover, the high affinity for Pgp may result in decreased intestinal absorption and blood-brain barrier penetration. Thus, further structural modifications of **13e** and **16a** should be performed to improve the permeability parameters and reduce the risk of DDI.

The metabolic stability was determined using human liver microsomes (HLMs). In general, compound **13e** was less metabolically stable (5 metabolites found, 41.8% remaining in the reaction mixture, Figure 6A) than **16a** (3 metabolites found, 74.8% remaining in the reaction mixture, Figure 6B). The most probable structures of the obtained *in vitro* metabolites were estimated using the MetaSite *in silico* tool and by MS and MS ion fragment analyses. The main metabolic pathways of both compounds were similar and were determined to occur via oxidation (for details see Figures S1-S3 in supplementary material). Another metabolic pathway of **16a** included the compound's defragmentation (M2), dehydrogenation and hydroxylation (M3). For compound **13e** additional reactions of defragmentation (M2), dehydrogenation and dealkylation (M4) were determined (for details see Figures S1-S3 in supplementary).

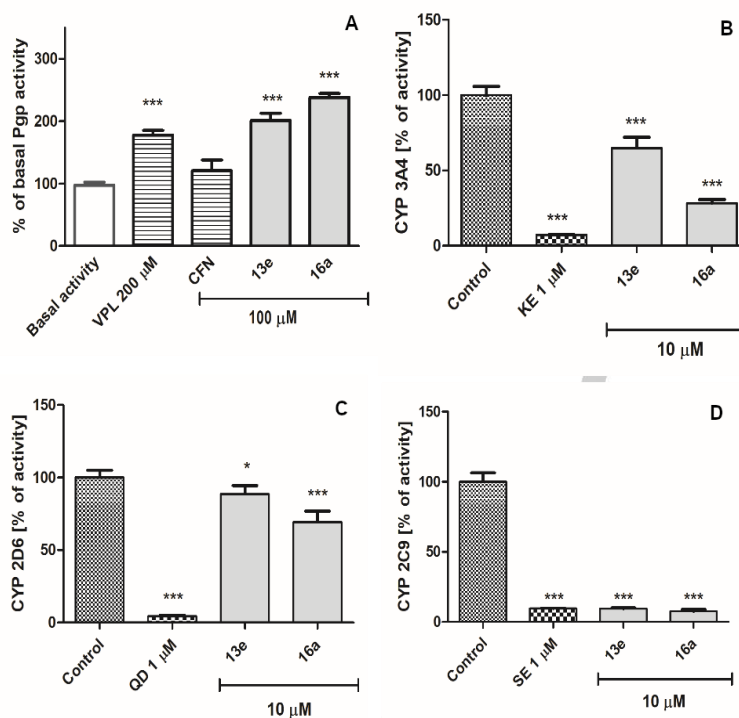


Figure 5 The effect of the Pgp substrate verapamil (VPL), Pgp negative compound caffeine (CFN) and tested ligands **13e**, **16a** (100 μ M) on Pgp basal activity (A). The effect of reference inhibitor ketoconazole and tested ligands **13e**, **16a** (10 μ M) on CYP3A4 (B), CYP2D6 (C) and CYP2C9 (D) activity. Statistical significance was evaluated by one-way ANOVA, followed by Bonferroni's comparison test (* $p < 0.05$, *** $p < 0.001$). Abbreviations: CFN – caffeine, VPL – verapamil, KE – ketoconazole, QD- quinidin, SE – sulfaphenazole.

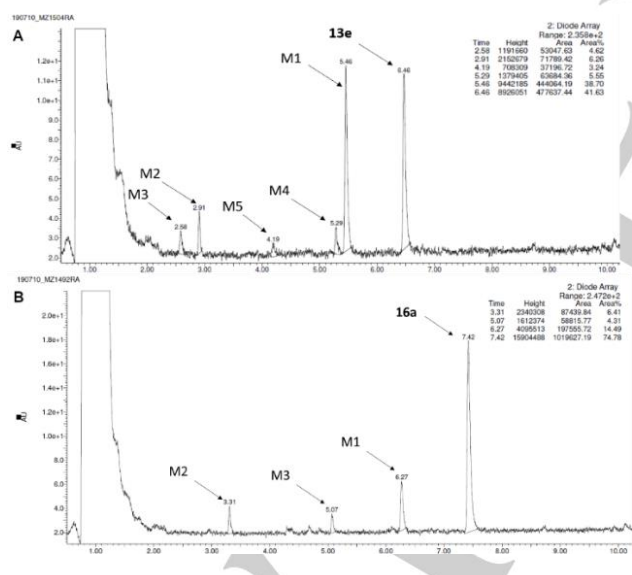


Figure 6 UPLC spectra of the reaction mixtures after 120 min incubation of compounds **13e** (A), **16a** (B) with HLMs.

Potential hepatotoxicity was examined in *hepatoma* HepG2 cells. The compounds were incubated with the cells for 72h. Compound **16a** showed higher hepatotoxic effects than **13e** with a statistically significant decrease in cells viability at 50 and 100 μ M (Figure 7A and 7B). However, the toxicity of compound **16a** should be considered as very weak in comparison to the reference compounds doxorubicin and CCCP (Figure 7B)

Docking studies

Adenosine A₁ and A_{2A} receptor docking studies

The recent publication of the human A₁ and A_{2A}AR crystal structures gave insights into the differences between A₁AR and A_{2A}AR binding modes for the A₁AR selective ligand PSB-36 (PDB ID: 5N2S and 5N2R respectively [42]) which was co-crystallized with both AR subtypes, located in the highly conserved orthosteric binding pockets. However, due to the relatively low A_{2A}AR affinity of PSB-36 ($K_i = 980$ nM [43]), along with well described proposed binding interactions of (annelated) xanthines [44], we used the 3REY crystal structure in complex with XAC for A_{2A}AR docking studies [45].

For all of the docked ligands, no valid poses were found in case of the A₁AR for the docking protocol used. This might be due to C2 carbonyl group calculated as the anchoring point for H-bonds with ASN254^{6,55}, that force a shift of the ligand placement toward TM2 in a narrow pocket formed by PHE171(EL2) and LEU250^{6,51}. Moreover, in comparison to PSB-36 co-crystallized within the binding pocket, the tricyclic core lacks a “free” proton at N5 position which is an important H-bond donor, therefore resulting in loss of one of the crucial interactions with ASN254^{6,55}.

FULL PAPER

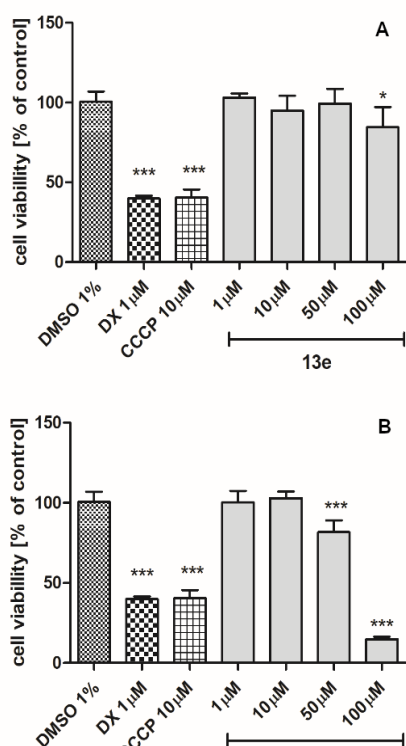


Figure 7 The effects of doxorubicin (DX, 1 μM), mitochondrial toxin carbonyl cyanide 3-chlorophenyl-hydrazone (CCCP, 10 μM) and compounds **13e** (A), **16a** (B) on *hepatoma* HepG2 cell line viability after 72 h of incubation. Statistical significance was evaluated by one-way ANOVA, followed by Bonferroni's comparison test (* $p < 0.05$, *** $p < 0.001$).

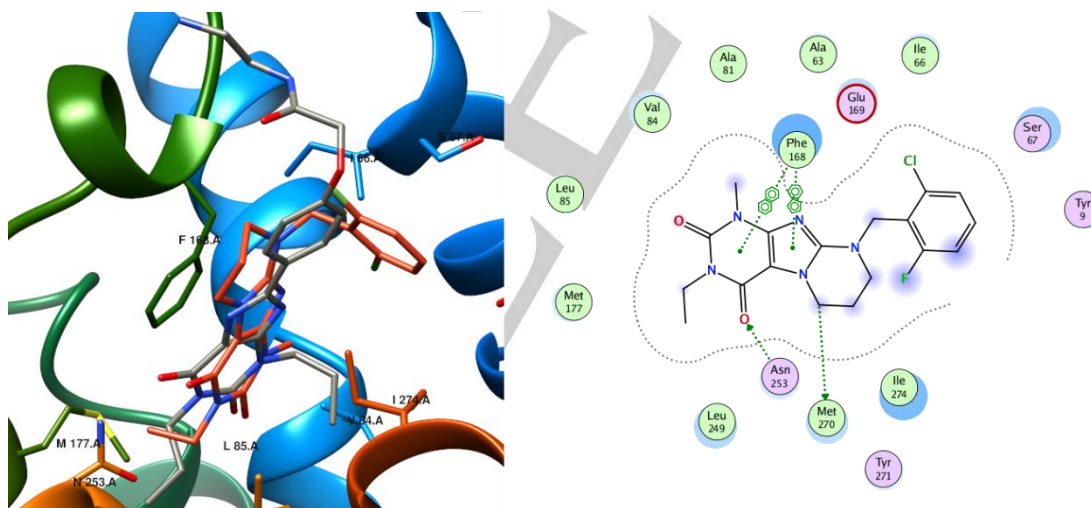


Figure 8 Calculated binding pose of **13e** (orange) and co-crystallized XAC (dark grey) in orthosteric binding pocket of $A_{2A}AR$ (3REY) with corresponding ligand interaction diagram (left and right panel respectively). ECL3 and partly TM7 residues were removed for better viewing clarity.

In case of the $A_{2A}AR$ similar putative interaction patterns for all of the docked ligands can be found. The terminal amino group of ASN253^{6,55} is suggested to form a key hydrogen bond with the carbonyl group in C4 of the purinedione. Annelated heterocyclic rings, independently of the size, are located in a narrow pocket formed by PHE168^{45,52}, that stabilizes the system through π - π stacking and GLU169 (ECL2) from one side, and TM7 amino

acids MET270^{7,35} and ILE 274^{7,39} from the other side, likely displaying hydrophobic interactions with both of these amino acids. *N*-3-alkyl substituents are predicted to occupy small a hydrophobic sub-pocket formed by LEU249^{6,51} and MET177^{5,38} on side, closed at the bottom by HIS250^{6,52}. Substituted benzyl moieties are probably placed in a subpocket between TM2, TM7 and TM1 stabilized by hydrophobic interactions with TYR271^{7,36} and TYR9^{1,35}. No additional interactions between halogen and/or alkyl(oxy) substituents of the benzyl moiety were found (Figure 8). The stability of the calculated poses was further evaluated by means of molecular dynamics simulations. Complexes appeared stable through the whole 600 ps simulation, retaining the key interactions, and the potential energy (U) of the atomic system at the level of ~ 1000 kcal/mol. Furthermore, during the simulation additional arene-H interactions of the substituted benzene ring with SER67^{2,65} and/or LEU267^{7,32} and TYR9^{1,35} were observed. In case of inactive derivatives (eg. **13d** and **20a**), either a rupture of the key hydrogen bond, or formation of a hydrogen bond with C2 carbonyl instead, followed by a shift of the purinedione core toward TM2 appeared.

MAO-B

Up to date, none of the MAO-B structures are co-crystallized with xanthine derivatives. Therefore, for the purpose of this study we used a 2V5Z structure with bound inhibitor safinamide (SAF, ^[46]), which shows some structural similarities (methylated amino-formamide fragment) to the purinedione core. Documented molecular docking studies carried out on the 8-styrylcaffeine structure, were an additional point during model selection ^[28]. The position of SAF within the binding pocket of 2V5Z is as follows: the halogen-substituted aromatic ring lies within the entry cavity, while the polar fragment is housed in an aromatic cage and is

directed towards the cofactor flavin adenine dinucleotide (FAD). Due to both, structural analogy to SAF and to recently described structures from our group ^[30], a similar arrangement was expected for the tested set of new ligands. In order to validate the methods used, SAF was redocked to its crystal structure, and the resulting pose was nearly perfectly superimposed with the native ligand with an RMSD value of 0.36.

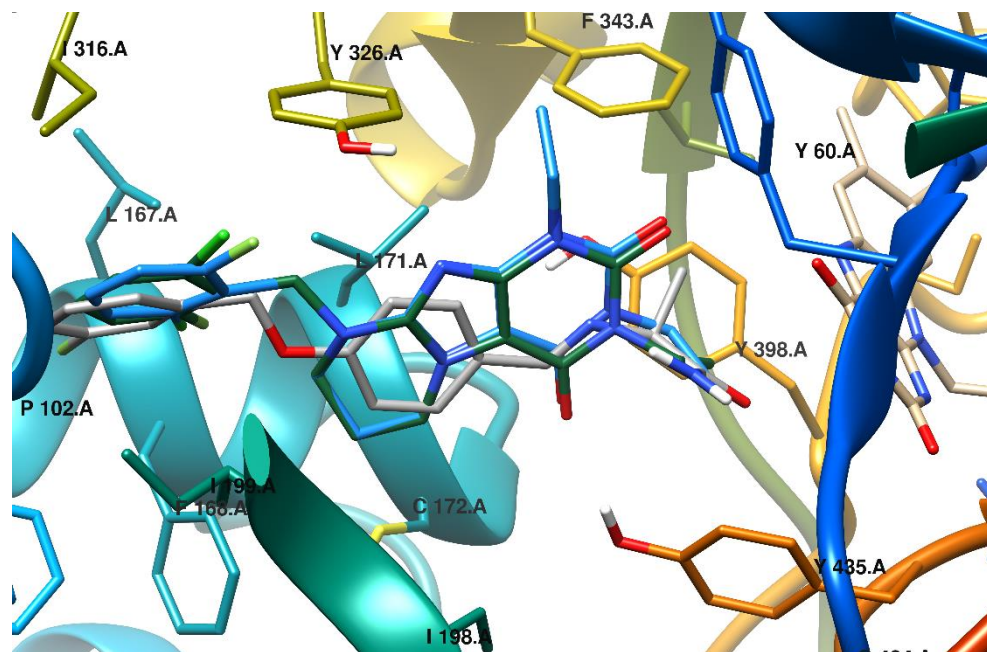


Figure 9. Putative binding modes of compounds **13e** (dark green) and **16b** (blue) as well as co-crystallized SAF (grey) in MAO-B active site. Residues 200-208 were removed for viewing clarity

Docking to a rigid form of the protein resulted in the presumed position of the tested set: for most of the ligands, the substituted phenyl moiety is pointing towards the entry cavity, while the purinedione core fits between the cage formed by TYR435 and GLN206 on one side, and TYR398 and LEU171 on the other side, which is in agreement with our previous findings. The N1-substituents of the annelated purinedione core point toward PHE343 and the core itself is stabilized by π - π stacking with TYR326 which is supposed to play an essential role for MAO-B inhibitor binding. Moreover, additional stabilization through halogen bonds between chlorine and the hydroxyl group of TYR326 was observed. Comparing the activity of homologous ligands, active **13e** (MZ1504) and inactive **16b** (MZ-1500), an ethyl substituent at the N1-position might induce a steric hindrance with TYR326 and/or PHE343 (Figure 9). Such an obstacle might also be the reason for the inactivity of azepane analogues, where the protonated nitrogen might clash with the LEU171 side chain, and force opposite, head-tail orientation for this subgroup of derivatives. Possible side chain and/or backbone conformational changes upon ligand binding into the active site were also tested using an induced fit protocol. Slight conformational changes resulted in the appearance of an additional protein-ligand interaction, through formation of an H-bond between the TYR435 hydroxyl group hydrogen and the N6 carbonyl oxygen for the most active ligands. In case of 7-membered annelated ring derivatives, obtained poses were either shifted toward the active site entrance and therefore removed from the aromatic cage and its possible interactions, or placed in a reversed manner (benzyl substituents facing FAD).

On the other hand, docking to a rigid form of the MAO-A crystal structure (PDB ID: 2Z5X^[47]) resulted in no valid docking poses for any of the ligands: all of the described compounds were subjected to docking. Poses for only 5 of the ligands were obtained, however with unacceptable orientation in MAO-A active site, resulting in a number of steric hindrances and lack of interactions.

Conclusion

In an attempt to further evaluate xanthine derivatives as potential anti-neurodegenerative agents, we designed, obtained and evaluated a series of *f*-bond annelated xanthine ligands with expected dual $A_{2A}AR$ /MAO-B inhibitory activity. For this purpose, a library of 19 novel compounds was obtained and biologically evaluated at the desired targets. Within this group we identified pyrimido [2,1-*f*]purinedione derived compounds **13e**, **14b**, **15b**, **16a** and **16b** as potent, selective $A_{2A}AR$ ligands, with affinity ranging from 207-504 nM. Additionally, compounds **13a**-**13f**, **14a** inhibited MAO-B with nanomolar IC_{50} values. Altogether, the obtained data indicate compound **13e** (9-(2-chloro-6-fluorobenzyl)-3-ethyl-1-methyl-6,7,8,9-tetrahydropyrimido[2,1-*f*]purine-2,4(1*H*,3*H*)-dione) to act as a dual compound ($A_{2A}AR$ K_i =264 nM, MAO-B IC_{50} =243 nM) and has therefore be potential for the treatment of PD and AD with expected symptomatic and neuroprotective effects. However, further structural modifications of **13e** in order to improve its ADMET properties are required. On the other hand, none of the diazepino[2,1-*f*]purinedione derivatives showed affinity for the investigated targets. Putative binding modes, and differences in activity were rationalized by molecular docking studies utilizing reported crystal structures.

Experimental Section

Chemistry

All commercially available reagents and solvents were used without further purification. Melting points (mp.) were determined on a MEL-TEMP II (LD Inc., USA) melting point apparatus and are uncorrected. ¹H NMR spectra were performed with a Varian Mercury-VX 300 MHz PFG spectrometer or a Bruker AMX 300 (Bruker, Germany) spectrometer in DMSO-*d*₆ or CDCl₃ with TMS as an internal standard. Chemical shifts were expressed in parts

FULL PAPER

per million (ppm). ^{13}C NMR data were recorded at 75 MHz on Varian-Mercury-VX 300 MHz PFG or 400 MHz spectrometer. The J values are reported in Hertz (Hz), and the splitting patterns are designated as follows: s (singlet), d (doublet), t (triplet), dd (doublet of doublets), dt (doublet of triplets), phe (phenyl), quin (quintet), m (multiplet). The purity of the final compounds was determined (%) on an Waters TQD mass spectrometer coupled with Waters ACQUITY UPLC system. Retention times (t_{R}) are given in minutes. Microwave reactions were performed in CEM Discover System microwave oven. Silica gel 60 (0.063–0.20 mm; Merck) was used for the column chromatography and the mixture of dichloromethane with methanol was applied as a mobile phase. TLC data were obtained using aluminium sheets coated with silica gel 60 F254 (Merck). Eluent system: DCM/MeOH 9:1, DCM/MeOH 9.5:0.5.

The synthesis and physicochemical properties of the compounds **11a-c** were reported previously^[46].

General procedure for the synthesis of pyrimido[2,1-*f*] purinedione (12-15b).

A mixture of 0.55 mmol of 8-bromo-7-(3-chloropropyl)theophylline **11a** or 8-bromo-7-(3-chloropropyl)-1-ethyl-3-methylxanthine **11b** or 8-bromo-7-(3-chloropropyl)-3-methyl-1-propylxanthine **11c** or 8-bromo-7-(3-chloropropyl)-3-methyl-1-(prop-2-ynyl)xanthine **11d**, or 8-bromo-7-(3-chloropropyl)-1,3-diethylxanthine **8b** 1.1 mmol of appropriate aromatic amine, 1.6 mmol of TEA and 1.00 ml of propanol was heated in closed vessels in microwave oven (300 Watt, Power Max Off, 160 °C, 10 bar) for 1 h. The solvent was removed and the residue was treated with ethanol. The products were purified by crystallization from ethanol or flash column chromatography over silica gel with CH_2Cl_2 : MeOH (100 : 0 to 80 : 20). The precipitate was filtered off and dried.

9-(3,4-dihydroxybenzyl)-1,3-dimethyl-6,7,8,9-tetrahydropyrimido[2,1-*f*]purine-2,4(1*H*,3*H*)-dione (12)

Yield: 39 mg; 35 %; mp: 216-218 °C; ^1H NMR (300 MHz, DMSO- d_6) δ ppm 2.01 (m, $J=5.27$ Hz, 2 H, C7H₂) 3.13 - 3.22 (m, 5 H, N3CH₃, C8H₂) 3.35 (s, 3 H, N1CH₃) 4.04 (t, $J=5.86$ Hz, 2 H, C6H₂) 4.49 (s, 2 H, N9CH₂) 6.52 - 6.59 (m, 1 H, C6H, phe) 6.63 - 6.72 (m, 2 H, C3H/C5H, phe) 8.86 (d, $J=11.72$ Hz, 2 H, 2 x OH); UPLC/MS purity 95.6 %, $t_{\text{R}} = 3.63$, C₁₇H₁₉N₅O₄, MW 357,37; [M+H]⁺ 358.21

9-(3-bromobenzyl)-3-ethyl-1-methyl-6,7,8,9-tetrahydropyrimido[2,1-*f*]purine-2,4(1*H*,3*H*)-dione (13a)

Yield: 138 mg; 60 %; mp: 178-180 °C; ^1H NMR (300 MHz, DMSO- d_6) δ ppm 1.06 (t, $J=7.03$ Hz, 3 H, CH₂CH₃) 1.99 - 2.10 (m, 2 H, C7H₂) 3.25 - 3.29 (m, 2 H, C8H₂) 3.33 (s, 3 H, N1CH₃) 3.84 (q, $J=7.03$ Hz, 2 H, N3CH₂) 4.07 (t, $J=5.86$ Hz, 2 H, C6H₂) 4.67 (s, 2 H, N9CH₂) 7.26 - 7.33 (m, 2 H, C5H/C6H, phe) 7.44 - 7.49 (m, 1 H, C2H, phe) 7.53 (s, 1 H, C4H, phe); ^{13}C NMR (DMSO- d_6) δ ppm: 13.8 (CH₃), 21.2 (C7), 29.7 (N1CH₃), 35.5 (N3CH₂), 41.8 (C6), 44.2 (C8), 51.9 (N9CH₂), 102.6 (C4a), 122.3 (C3, phe), 127.1 (C6, phe), 130.7 (C5, phe), 130.9 (C4, phe), 131.2 (C2, phe), 140.5 (C1, phe), 148.6 (C10a), 151.0 (C9a), 151.8 (C2), 152.8 (C4). UPLC/MS purity 96.31 %, $t_{\text{R}} = 6.72$, C₁₈H₂₀BrN₅O₂, MW 418,30, [M+H]⁺ 420.27.

9-(2-chlorobenzyl)-3-ethyl-1-methyl-6,7,8,9-tetrahydropyrimido[2,1-*f*]purine-2,4(1*H*,3*H*)-dione (13b)

Yield: 117 mg; 57 %; mp: 178-180 °C; ^1H NMR (300 MHz, DMSO- d_6) δ ppm 1.07 (t, $J=7.03$ Hz, 3 H, CH₂CH₃) 2.05 - 2.14 (m, 2 H, C7H₂) 3.29 (s, 3 H, N1CH₃) 3.33 - 3.36 (m, 2 H, C8H₂) 3.84 (q, $J=6.84$ Hz, 2 H, N3CH₂) 4.12 (t, $J=5.86$ Hz, 2 H, C6H₂) 4.76 (s, 2 H, N9CH₂) 7.29 - 7.36 (m, 3 H, C3H/C4H/C5H, phe) 7.44 - 7.50 (m, 1 H, C6H, phe); ^{13}C NMR (DMSO- d_6) δ ppm: 13.8 (CH₃), 21.2 (C7), 29.8 (N1CH₃), 35.5 (N3CH₂), 41.9 (C6), 44.7 (C8), 50.5 (N9CH₂), 104.1 (C4a), 127.9 (C4, phe), 129.2 (C6, phe), 129.5 (C5, phe), 130.0 (C3, phe), 132.8 (C2, phe), 134.8 (C1, phe), 148.6 (C10a),

151.0 (C9a), 152.8 (C2), 153.0 (C4). UPLC/MS purity 95.63 %, $t_{\text{R}} = 6.56$, C₁₈H₂₀ClN₅O₂, MW 373,84, [M+H]⁺ 374.16.

9-(3,4-dichlorobenzyl)-3-ethyl-1-methyl-6,7,8,9-tetrahydropyrimido[2,1-*f*]purine-2,4(1*H*,3*H*)-dione (13c)

Yield: 116 mg; 52 %; mp: 178-180 °C; ^1H NMR (300 MHz, DMSO- d_6) δ ppm 1.06 (t, $J=7.03$ Hz, 3 H, CH₂CH₃) 2.00 - 2.09 (m, 2 H, C7H₂) 3.26 - 3.29 (m, 2 H, C8H₂) 3.32 (s, 3 H, N1CH₃) 3.84 (q, $J=7.03$ Hz, 2 H, N3CH₂) 4.07 (t, $J=6.15$ Hz, 2 H, C6H₂) 4.66 (s, 2 H, N9CH₂) 7.31 (dd, $J=8.21$, 1.76 Hz, 1 H, C6H, phe) 7.56 - 7.61 (m, 2 H, C2H/C5H, phe); ^{13}C NMR (DMSO- d_6) δ ppm: 13.8 (CH₃), 21.2 (C7), 29.7 (N1CH₃), 35.5 (N3CH₂), 41.8 (C6), 44.3 (C8), 51.4 (N9CH₂), 102.7 (C4a), 128.5 (C6, phe), 130.2 (C5, phe), 130.4 (C2, phe), 131.2 (C3, phe), 131.5 (C4, phe), 134.0 (C1, phe), 148.6 (C10a), 151.0 (C9a), 151.7 (C2), 152.8 (C4). UPLC/MS purity 96.83 %, $t_{\text{R}} = 7.18$, C₁₈H₁₉Cl₂N₅O₂, MW 408,28, [M+H]⁺ 408.30.

9-(3,5-dichlorobenzyl)-3-ethyl-1-methyl-6,7,8,9-tetrahydropyrimido[2,1-*f*]purine-2,4(1*H*,3*H*)-dione (13d)

Yield: 110 mg; 49 %; mp: 198-199 °C; ^1H NMR (500 MHz, DMSO- d_6) δ ppm 1.04 (d, $J=5.73$ Hz, 3 H, NCH₂CH₃) 2.04 (br. s., 2 H, C7H₂) 3.29 - 3.32 (m, 5 H, C8H₂, N1CH₃) 3.79 - 3.86 (m, 2 H, N3CH₂) 4.00 - 4.10 (m, 2 H, C6H₂) 4.58 - 4.70 (m, 2 H, N9CH₂) 7.36 (br. s., 2 H, C1H/C6H, phe) 7.50 (br. s., 1 H, C4H, phe) UPLC/MS purity 95.96 %, $t_{\text{R}} = 7.39$, C₁₈H₁₉Cl₂N₅O₂, MW 408,28, [M+H]⁺ 408.30.

9-(2-chloro-6-fluorobenzyl)-3-ethyl-1-methyl-6,7,8,9-tetrahydropyrimido[2,1-*f*]purine-2,4(1*H*,3*H*)-dione (13e)

Yield: 120 mg; 56 %; mp: 180-181 °C; ^1H NMR (300 MHz, CHLOROFORM-*d*) δ ppm 1.18 - 1.25 (m, 3 H, CH₂CH₃) 2.08 (quin, $J=5.71$ Hz, 2 H, C7H₂) 3.19 - 3.25 (m, 2 H, C8H₂) 3.51 (s, 3 H, N1CH₃) 4.03 (q, $J=6.64$ Hz, 2 H, N3CH₂) 4.20 (t, $J=5.86$ Hz, 2 H, C6H₂) 4.92 (d, $J=1.76$ Hz, 2 H, N9CH₂) 6.98 - 7.07 (m, 1 H, C4H, phe) 7.19 - 7.31 (m, 2 H, C3H/C5H, phe); ^{13}C NMR (CHLOROFORM-*d*) δ ppm: 13.5 (CH₃), 21.4 (C7), 29.6 (N1CH₃), 36.01 (N3CH₂), 41.6 (C6), 43.4 (C8), 44.1 (d, $^3J_{\text{C,F}} = 3.4$ Hz, N9CH₂), 103.1 (C4a), 114.3 (d, $^2J_{\text{C,F}} = 23.1$ Hz, C5, phe), 121.9 (d, $^2J_{\text{C,F}} = 17.3$ Hz, C1, phe), 125.7 (d, $^4J_{\text{C,F}} = 3.4$ Hz, C3, phe), 130.0 (d, $^3J_{\text{C,F}} = 10.3$ Hz, C4, phe), 136.2 (d, $^3J_{\text{C,F}} = 5.8$ Hz, C2, phe), 148.7 (C10a), 151.3 (C9a), 151.5 (C2), 153.7 (C4), 162.3 (d, $^1J_{\text{C,F}} = 251.1$ Hz, C6, phe). UPLC/MS purity 97.77 %, $t_{\text{R}} = 6.46$, C₁₈H₁₉ClF₂N₅O₂, MW 391,83, [M+H]⁺ 392.17.

9-(2-chloro-3,6-difluorobenzyl)-3-ethyl-1-methyl-6,7,8,9-tetrahydropyrimido[2,1-*f*]purine-2,4(1*H*,3*H*)-dione (13f)

Yield: 92 mg; 41 %; mp: 165-167 °C; ^1H NMR (300 MHz, DMSO- d_6) δ ppm 1.02 - 1.09 (m, 3 H, CH₂CH₃) 1.96 - 2.05 (m, 2 H, C7H₂) 3.21 - 3.27 (m, 2 H, C8H₂) 3.31 (s, 3 H, N1CH₃) 3.82 (q, $J=6.64$ Hz, 2 H, N3CH₂) 4.03 (t, $J=5.86$ Hz, 2 H, C6H₂) 4.79 (d, $J=1.17$ Hz, 2 H, N9CH₂) 7.27 - 7.36 (m, 1 H, C4H, phe) 7.47 (td, $J=8.79$, 4.69 Hz, 1 H, C5H, phe); ^{13}C NMR (DMSO- d_6) δ ppm: 13.8 (CH₃), 21.3 (C7), 29.6 (N1CH₃), 35.5 (N3CH₂), 41.8 (C6), 44.3 (C8), 44.52 (N9CH₂), 102.6 (C4a), 115.8 (dd, $^2J_{\text{C,F}} = 33.4$ Hz, $^3J_{\text{C,F}} = 17.8$ Hz, C5, phe), 117.4 (dd, $^2J_{\text{C,F}} = 33.4$ Hz, $^3J_{\text{C,F}} = 13.8$ Hz, C4, phe), 123.4 (dd, $^2J_{\text{C,F}} = 46$ Hz, $^3J_{\text{C,F}} = 18.4$ Hz, C1, phe), 148.4 (C10a), 151.0 (C9a), 151.5 (C2), 152.9 (C4), 154.7 (dd, $^4J_{\text{C,F}} = 4.6$ Hz, $^1J_{\text{C,F}} = 260.3$ Hz, C3, phe), 157.86 (dd, $^4J_{\text{C,F}} = 2.3$ Hz, $^1J_{\text{C,F}} = 252.2$ Hz, C6, phe). UPLC/MS purity 96.88 %, $t_{\text{R}} = 6.51$, C₁₈H₁₈ClF₂N₅O₂, MW 409,82, [M+H]⁺ 410.30.

9-(2-chlorobenzyl)-1-methyl-3-propyl-6,7,8,9-tetrahydropyrimido[2,1-*f*]purine-2,4(1*H*,3*H*)-dione (14a)

Yield: 96 mg; 45 %; mp: 194-195 °C; ^1H NMR (300 MHz, DMSO- d_6) δ ppm 0.82 (t, $J=7.60$ Hz, 3 H, CH₃) 1.50 (sxt, $J=7.38$ Hz, 2 H, N3CH₂CH₂) 2.05 - 2.14 (m, 2 H, C7H₂) 3.28 (s, 3 H, N1CH₃) 3.32 - 3.36 (m, 2 H, C8H₂) 3.75 (t, $J=7.30$ Hz, 2 H, N3CH₂) 4.11 (t, $J=5.57$ Hz, 2 H, C6H₂) 4.75 (s, 2 H, N9CH₂) 7.28 - 7.37 (m, 3 H, C3H/C4H/C5H, phe) 7.43 - 7.49 (m, 1 H, C6H,

FULL PAPER

phe)¹³C NMR (DMSO-*d*₆) δ ppm: 11.7 (CH₃), 21.2 (CH₂), 21.4 (C7), 29.8 (N1CH₃), 41.9 (N3CH₂), 42.0 (C6), 44.7 (C8), 50.5 (N9CH₂), 102.6 (C4a), 127.9 (C4, phe), 129.2 (C6, phe), 129.5 (C5, phe), 129.9 (C3, phe), 132.7 (C2, phe), 134.8 (C1, phe), 148.6 (C10a), 151.2 (C9a), 151.8 (C2), 153.0 (C4). UPLC/MS purity 95.74 %, *t*_R = 7.08, C₁₉H₂₂ClN₅O₂, MW 387.87, [M+H]⁺ 388.18.

9-(2-chloro-6-fluorobenzyl)-1-methyl-3-propyl-6,7,8,9-tetrahydropyrimido[2,1-*f*]purine-2,4(1*H*,3*H*)-dione (14b)

Yield: 125 mg; 57 %; mp: 157-158 °C; ¹H NMR (300 MHz, DMSO-*d*₆) δ ppm 0.81 (t, *J* = 7.33 Hz, 3 H, CH₂CH₃) 1.42 - 1.56 (m, 2 H, N3CH₂CH₂) 1.95 - 2.03 (m, 2 H, C7H₂) 3.20 (t, *J* = 5.57 Hz, 2 H, C8H₂) 3.32 (s, 3 H, N1CH₃) 3.70 - 3.77 (m, 2 H, N3CH₂) 4.03 (t, *J* = 6.15 Hz, 2 H, C6H₂) 4.78 (s, 2 H, N9CH₂) 7.20 - 7.28 (m, 1 H, C4H, phe) 7.32 - 7.45 (m, 2 H, C3H/C5H, phe); ¹³C NMR (DMSO-*d*₆) δ ppm: 11.64 (CH₃), 21.3 (CH₂), 21.4 (C7), 29.7 (N1CH₃), 41.9 (d, ³*J*_{C,F} = 11.5 Hz, N9CH₂), 43.9 (C6), 44.4 (N3CH₂), 45.9 (C8), 102.5 (C4a), 115.1 (d, ²*J*_{C,F} = 23 Hz, C5, phe), 121.4 (d, ²*J*_{C,F} = 17.3 Hz, C1, phe), 126.2 (d, ⁴*J*_{C,F} = 3.4 Hz, C3, phe), 131.1 (d, ³*J*_{C,F} = 10.4 Hz, C4, phe), 135.6 (d, ³*J*_{C,F} = 5.7 Hz, C2, phe), 148.5 (C10a), 151.2 (C9a), 151.6 (C2), 153.1 (C4), 160.5 (C6, phe). UPLC/MS purity 97.21 %, *t*_R = 6.97, C₁₉H₂₁ClFN₅O₂, MW 405.86, [M+H]⁺ 406.19.

9-(2-chlorobenzyl)-1-methyl-3-(prop-2-yn-1-yl)-6,7,8,9-tetrahydropyrimido[2,1-*f*]purine-2,4(1*H*,3*H*)-dione (15a)

Yield: 99 mg; 47 %; mp: 230-232 °C; ¹H NMR (300 MHz, DMSO-*d*₆) δ ppm 2.06 - 2.15 (m, 2 H, C7H₂) 3.03 (t, *J* = 2.34 Hz, 1 H, C≡CH) 3.30 (s, 3 H, N1CH₃) 3.35 (m, 2 H, C8H₂) 4.12 (t, *J* = 5.86 Hz, 2 H, C6H₂) 4.53 (d, *J* = 2.34 Hz, 2 H, N3CH₂) 4.77 (s, 2 H, N9CH₂) 7.28 - 7.38 (m, 3 H, C3H/C4H/C5H, phe) 7.44 - 7.50 (m, 1 H, C6H, phe); ¹³C NMR (DMSO-*d*₆) δ ppm: 21.1 (C7), 29.9 (N1CH₃), 30.0 (N3CH₂), 41.9 (C6), 44.7 (C8), 50.5 (N9CH₂), 72.9 (C≡CH), 80.5 (C≡CH), 102.4 (C4a), 127.9 (C4, phe), 129.3 (C6, phe), 129.5 (C5, phe), 130.0 (C3, phe), 132.8 (C2, phe), 134.7 (C1, phe), 149.0 (C10a), 150.65 (C9a), 151.9 (C2), 152.0 (C4). UPLC/MS purity 96.71 %, *t*_R = 6.60, C₁₉H₁₈ClN₅O₂, MW 383.84, [M+H]⁺ 384.13.

9-(2-chloro-6-fluorobenzyl)-1-methyl-3-(prop-2-yn-1-yl)-6,7,8,9-tetrahydropyrimido[2,1-*f*]purine-2,4(1*H*,3*H*)-dione (15b)

Yield: 137 mg; 62 %; mp: 216-218 °C; ¹H NMR (500 MHz, DMSO-*d*₆) δ ppm 1.98 (br. s., 2 H, C7H₂) 3.00 (br. s., 1 H, C≡CH) 3.19 (br. s., 2 H, C8H₂) 3.32 (s, 3 H, N1CH₃) 4.01 (t, *J* = 5.44 Hz, 2 H, C6H₂) 4.49 (br. s., 2 H, N3CH₂) 4.78 (s, 2 H, N9CH₂) 7.20 - 7.25 (m, 1 H, C4H, phe) 7.31 - 7.35 (m, 1 H, C3H, phe) 7.36 - 7.41 (m, 1 H, C5H, phe); ¹³C NMR (DMSO-*d*₆) δ ppm: 21.3 (C7), 29.9 (N1CH₃), 30.0 (N3CH₂), 41.9 (C6), 44.0 (C8), 44.5 (d, ³*J*_{C,F} = 3.0 Hz, N9CH₂), 73.0 (C≡CH), 80.6 (C≡CH), 102.4 (C4a), 115.2 (d, ²*J*_{C,F} = 22.3 Hz, C5, phe), 122.4 (d, ²*J*_{C,F} = 17.5 Hz, C1, phe), 126.3 (d, ⁴*J*_{C,F} = 3.1 Hz, C3, phe), 131.3 (d, ³*J*_{C,F} = 9.6 Hz, C4, phe), 135.7 (d, ³*J*_{C,F} = 6.0 Hz, C2, phe), 149.0 (C10a), 150.8 (C9a), 151.9 (C2), 152.0 (C4), 160.5 (C6, phe). UPLC/MS purity 95.99 %, *t*_R = 6.48, C₁₉H₁₇ClFN₅O₂, MW 401.83, [M+H]⁺ 402.14.

9-(2-bromobenzyl)-1,3-diethyl-6,7,8,9-tetrahydropyrimido[2,1-*f*]purine-2,4(1*H*,3*H*)-dione (16a)

Yield: 126 mg; 53 %; mp: 145-147 °C; ¹H NMR (300 MHz, CHLOROFORM-*d*) δ ppm 1.26 (dt, *J* = 18.17, 7.03 Hz, 6 H, 2 x CH₂CH₃) 2.15 (dt, *J* = 11.72, 5.86 Hz, 2 H, C7H₂) 3.30 - 3.35 (m, 2 H, C8H₂) 4.00 - 4.12 (m, 4 H, CH₂CH₃) 4.25 (t, *J* = 5.86 Hz, 2 H, C6H₂) 4.86 (s, 2 H, N9CH₂) 7.13 - 7.20 (m, 1 H, C5H, phe) 7.27 - 7.38 (m, 2 H, C6H/C4H, phe) 7.58 (dd, *J* = 7.62, 1.17 Hz, 1 H, C3H, phe); ¹³C NMR (CHLOROFORM-*d*) δ ppm: 13.4 (N3CH₂CH₃), 13.5 (N1CH₂CH₃), 21.5 (C7), 36.0 (N3CH₂), 38.3 (N1CH₂), 41.7 (C6), 44.3 (C8), 52.7 (N9CH₂), 103.3 (C4a), 123.8 (C2, phe), 127.7 (C5, phe), 129.2 (C4, phe), 129.6 (C6, phe), 133.0 (C3, phe), 136.0 (C1, phe), 148.3 (C10a), 150.6 (C9a), 151.7 (C2), 153.8 (C4). UPLC/MS purity 99.43 %, *t*_R = 7.41, C₁₉H₂₂BrN₅O₂, MW 432.32, [M+H]⁺ 434.18.

9-(2-chloro-6-fluorobenzyl)-1,3-diethyl-6,7,8,9-tetrahydropyrimido[2,1-*f*]purine-2,4(1*H*,3*H*)-dione (16b)

Yield: 136 mg; 61 %; mp: 162-163 °C; ¹H NMR (500 MHz, DMSO-*d*₆) δ ppm 1.03 (t, *J* = 7.16 Hz, 3 H, N3CH₂CH₃) 1.11 (t, *J* = 7.16 Hz, 3 H, N1CH₂CH₃) 1.95 - 2.01 (m, 2 H, C7H₂) 3.20 - 3.24 (m, 2 H, C8H₂) 3.80 (q, *J* = 6.87 Hz, 2 H, N3CH₂) 3.89 (q, *J* = 7.26 Hz, 2 H, N1CH₂) 4.01 (t, *J* = 6.01 Hz, 2 H, C6H₂) 4.75 (s, 2 H, N9CH₂) 7.18 - 7.23 (m, 1 H, C4H, phe) 7.29 - 7.32 (m, 1 H, C3H, phe) 7.34 - 7.39 (m, 1 H, C5H, phe); ¹³C NMR (CHLOROFORM-*d*) δ ppm: 13.7 (N3CH₂CH₃), 13.9 (N1CH₂CH₃), 21.4 (C7), 35.5 (N3CH₂), 38.1 (N1CH₂), 41.8 (C6), 44.3 (C8), 44.6 (d, ³*J*_{C,F} = 3.0 Hz, N9CH₂), 102.7 (C4a), 115.1 (d, ²*J*_{C,F} = 22.9 Hz, C5, phe), 122.7 (d, ²*J*_{C,F} = 17.5 Hz, C1, phe), 126.2 (d, ⁴*J*_{C,F} = 3.0 Hz, C3, phe), 131.1 (d, ³*J*_{C,F} = 9.7 Hz, C4, phe), 135.7 (d, ³*J*_{C,F} = 5.4 Hz, C2, phe), 148.0 (C10a), 150.6 (C9a), 151.7 (C2), 152.9 (C4), 162.3 (d, ¹*J*_{C,F} = 249.3 Hz, C6, phe). UPLC/MS purity 98.12 %, *t*_R = 7.14, C₁₉H₂₁ClFN₅O₂, MW 405.86, [M+H]⁺ 406.19.

7-(3-Bromopropyl)-8-(hydroxymethyl)-1,3-dimethyl-1*H*-purine-2,6(3*H*,7*H*)-dione (18)

8-(hydroxymethyl)-1,3-dimethyl-1*H*-purine-2,6(3*H*,7*H*)-dione (17) (2.10 g, 10.0 mmol) was dissolved in DMF (20 mL), and potassium carbonate (4.15 g, 30.0 mmol) and 1,3-dibromopropane (6.06 g, 30.0 mmol) were added. The solution was stirred for 5 h at 110 °C. Then, the volatiles were removed in vacuo and the residue was purified by flash chromatography (silica gel, CH₂Cl₂/MeOH 19:1). Yield: 2.12 g, 65%; mp: 203 °C;

General procedure for tetrahydrodiazepino [2,1-*f*]purinediones (20a-f)

According to a previously published procedure [49] 7-(3-bromopropyl)-8-(hydroxymethyl)-1,3-dimethyl-1*H*-purine-2,6(3*H*,7*H*)-dione (18) (2.20 g, 6.71 mmol) was dissolved in CH₂Cl₂ (60 mL) and cooled to 0 °C. A solution of PBr₃ (2.00 mL, 20.7 mmol) in CH₂Cl₂ (40 mL) was added dropwise. The solution was allowed to warm to room temperature and stirred for 1 h. Then it was cooled again to 0 °C and excess PBr₃ was hydrolysed by addition of saturated aqueous NaHCO₃ (25 mL). The organic layer was then separated, and the aqueous layer extracted with CH₂Cl₂ (2x50 mL). The combined organic extracts were dried (MgSO₄) and the solvent was evaporated in vacuo. The crude 7-(3-bromopropyl)-8-(bromomethyl)-1,3-dimethylpurine-2,4-dione (19) was divided for six equal parts and used directly in the next step. Compound 19 (~1.00 mmol), the appropriate amine (2.00 mmol), n-propanol (2 ml) and TEA (0.4 ml) were heated in a microwave reactor (300 Watt, Power Max On, 150 °C, 10 bar) for 1 h. The solvent was removed under reduced pressure and the residue was purified by flash chromatography (dichloromethane: methanol 9:1).

9-benzyl-1,3-dimethyl-7,8,9,10-tetrahydro-1*H*-[1,4]diazepino[2,1-*f*]purine-2,4(3*H*,6*H*)-dione(20a)

Yield: 278 mg, 82.1 %; mp: 195-196 °C; ¹H NMR (400 MHz, DMSO-*d*₆) δ ppm 1.85 (br. s., 2 H, C7H₂), 3.00 - 3.05 (m, 2 H, C8H₂), 3.23 (s, 3 H, N3CH₃), 3.40 (s, 3 H, N1CH₃), 3.55 (s, 2 H, C10H₂), 3.96 (s, 2 H, N9CH₂), 4.58 - 4.63 (m, 2 H, C6H₂), 7.26 - 7.34 (m, 5 H, phe); ¹³C NMR (DMSO-*d*₆) δ ppm: 25.24 (C7), 28.00 (N3CH₃), 29.89 (N1CH₃), 45.19 (C6), 52.13 (C10), 56.35 (N9CH₂), 57.91 (C8), 107.14 (C4a), 127.55 (C4, phe), 128.70 (C3, C5, phe), 129.23 (C2, C6, phe), 138.77 (C1, phe), 147.13 (C11a), 151.37 (C2), 154.40 (C4), 155.03 (C10a); UPLC/MS purity 99.45 %, *t*_R = 3.04, C₁₈H₂₁N₅O₂, MW 339.39, [M+H]⁺ 340.13.

9-(2-chlorobenzyl)-1,3-dimethyl-7,8,9,10-tetrahydro-1*H*-[1,4]diazepino[2,1-*f*]purine-2,4(3*H*,6*H*)-dione (20b)

Yield: 248 mg, 66.2 %; mp 156-157 °C; ¹H NMR (400 MHz, DMSO-*d*₆) δ ppm 1.89 (br. s., 2 H, C7H₂), 3.06 - 3.10 (m, 2 H, C8H₂), 3.22 (s, 3 H, N3CH₂), 3.40 (s, 3 H, N1CH₂), 3.60 (s, 2 H, C10H₂), 4.00 (s, 2 H, N9CH₂),

FULL PAPER

4.59 - 4.66 (m, 2 H, C6H₂), 7.32 (td, *J*=7.14, 1.76 Hz, 2 H, C4H, C5H, phe), 7.41 - 7.48 (m, 2 H, C3H, C6H, phe); ¹³C NMR (DMSO-*d*₆) δ ppm: 25.21 (C7), 28.01 (N3CH₃), 29.91 (N1CH₃), 45.17 (C6), 51.94 (C10), 54.39 (N9CH₂), 56.44 (C8), 107.19 (C4a), 127.50 (C5, phe), 129.33 (C3, phe), 129.85 (C4, phe), 131.38 (C6, phe), 133.93 (C2, phe), 136.18 (C1, phe), 147.14 (C11a), 151.36 (C2), 154.30 (C4), 155.03 (C10a); UPLC/MS purity 95.58 %, *t*_R = 4.60, C₁₈H₂₀ClN₅O₂, MW 373.84, [M+H]⁺ 374.09.

9-(3-chlorobenzyl)-1,3-dimethyl-7,8,9,10-tetrahydro-1H-[1,4]diazepino[2,1-*f*]purine-2,4(3*H*,6*H*)-dione (20c)

Yield: 270 mg, 72.4 %; mp: 168-169 °C; ¹H NMR (400 MHz, DMSO-*d*₆) δ ppm 1.85 (br. s., 2 H, C7H₂), 3.02 - 3.08 (m, 2 H, C8H₂), 3.22 (s, 3 H, N3CH₂), 3.39 (s, 3 H, N1CH₂), 3.55 (s, 2 H, C10H₂), 3.96 (s, 2 H, N9CH₂), 4.56 - 4.65 (m, 2 H, C6H₂), 7.22 - 7.29 (m, 1 H, C2H, phe), 7.31 - 7.41 (m, 3 H, C4H, C5H, C6H, phe); ¹³C NMR (DMSO-*d*₆) δ ppm: 25.04 (C7), 27.99 (N3CH₃), 29.86 (N1CH₃), 45.16 (C6), 51.92 (C10), 56.35 (N9CH₂), 56.83 (C8), 107.17 (C4a), 127.51 (C5, phe), 127.85 (C6, phe), 128.98 (C4, phe), 130.55 (C2, phe), 133.41 (C3, phe), 141.50 (C1, phe), 147.11 (C11a), 151.34 (C2), 154.27 (C4), 155.01 (C10a); UPLC/MS purity 100.0 %, *t*_R = 4.21, C₁₈H₂₀ClN₅O₂, MW 373.83, [M+H]⁺ 374.16

9-(4-chlorobenzyl)-1,3-dimethyl-7,8,9,10-tetrahydro-1H-[1,4]diazepino[2,1-*f*]purine-2,4(3*H*,6*H*)-dione (20d)

Yield: 294 mg, 78.7 %; mp: 224-225 °C; ¹H NMR (500 MHz, CHLOROFORM-*d*) δ ppm 1.92 (br. s., 2 H, C7H₂), 3.05 - 3.08 (m, 2 H, C8H₂), 3.39 (s, 3 H, N3CH₂), 3.54 (s, 3 H, N1CH₂), 3.56 (s, 2 H, C10H₂), 3.97 (s, 2 H, N9CH₂), 4.62 - 4.68 (m, 2 H, C6H₂), 7.20 - 7.23 (m, 2 H, C2H, C6H, phe), 7.26 - 7.29 (m, 2 H, C3H, C5H, phe); ¹³C NMR (CHLOROFORM-*d*) δ ppm: 25.80 (C7), 28.03 (N3CH₃), 29.83 (N1CH₃), 45.43 (C6), 52.73 (C10), 56.66 (N9CH₂), 57.91 (C8), 107.67 (C4a), 128.74 (C2, C3, C5, C6 phe), 130.23 (C1, C4, phe), 147.37 (C11a), 151.69 (C2), 155.51 (C4, C10a); UPLC/MS purity 95.97 %, *t*_R = 4.59, C₁₈H₂₀ClN₅O₂, MW 373.83, [M+H]⁺ 374.16

9-(3,4-dichlorobenzyl)-1,3-dimethyl-7,8,9,10-tetrahydro-1H-[1,4]diazepino[2,1-*f*]purine-2,4(3*H*,6*H*)-dione (20e)

Yield: 230 mg, 56.2 %; mp: 213-215 °C; ¹H NMR (500 MHz, CHLOROFORM-*d*) δ ppm 1.92 (t, *J*=4.01 Hz, 2 H, C7H₂), 3.06 - 3.11 (m, 2 H, C8H₂), 3.39 (s, 3 H, N3CH₂), 3.53 (s, 2 H, C10H₂), 3.54 (s, 3 H, N1CH₂), 3.96 (s, 2 H, N9CH₂), 4.63 - 4.68 (m, 2 H, N9CH₂), 7.12 (dd, *J*=8.02, 1.72 Hz, 1 H, C6H, phe), 7.37 (d, *J*=8.59 Hz, 1 H, C5H, phe), 7.39 (d, *J*=1.72 Hz, 1 H, C2H, phe); ¹³C NMR (CHLOROFORM-*d*) δ ppm: 25.48 (C7), 28.03 (N3CH₃), 29.83 (N1CH₃), 45.42 (C6), 52.51 (C10), 56.89 (N9CH₂), 57.28 (C8), 107.69 (C4a), 128.09 (C3, C6, phe), 130.53 (C5, phe), 130.75 (C2, phe), 131.49 (C4, phe), 132.66 (C1, phe), 147.36 (C11a), 151.68 (C2), 155.51 (C4, C10a); UPLC/MS purity 100.00 %, *t*_R = 6.35, C₁₈H₁₉Cl₂N₅O₂, MW 408.28, [M+]⁺ 408.06.

9-(2,4-dichlorobenzyl)-1,3-dimethyl-7,8,9,10-tetrahydro-1H-[1,4]diazepino[2,1-*f*]purine-2,4(3*H*,6*H*)-dione (20f)

Yield: 211 mg, 51.7 %; mp: 233-234 °C; ¹H NMR (500 MHz, CHLOROFORM-*d*) δ ppm 1.96 (br. s., 2 H, C7H₂), 3.10 - 3.17 (m, 2 H, C8H₂), 3.39 (s, 3 H, N3CH₂), 3.54 (s, 3 H, N1CH₂), 3.64 (s, 2 H, C10H₂), 4.00 (s, 2 H, N9CH₂), 4.64 - 4.71 (m, 2 H, C6H₂), 7.22 (dd, *J*=8.02, 2.29 Hz, 1 H, C6H, phe), 7.35 (d, *J*=2.29 Hz, 1 H, C5H, phe), 7.36 - 7.41 (m, 1 H, C3H, phe); ¹³C NMR (CHLOROFORM-*d*) δ ppm: 25.61 (C7), 28.03 (N3CH₃), 29.84 (N1CH₃), 45.43 (C6), 52.47 (C10), 54.27 (N9CH₂), 56.91 (C8), 107.74 (C4a), 127.28 (C5, phe), 129.55 (C3, phe), 131.57 (C6 phe), 135.00 (C1, C2, C4, phe), 147.38 (C11a), 151.68 (C2), 155.52 (C4, C10a); UPLC/MS purity 96.43 %, *t*_R = 5.70, C₁₈H₁₉Cl₂N₅O₂, MW 408.28, [M+]⁺ 408.06

Biological evaluation

Radioligand binding assays at adenosine receptors

AR radioligand binding assays were performed as previously described^[30]. HEK or CHO cells recombinantly expressing the respective human AR subtype were purchased from PerkinElmer. The following compounds were employed as radioligands: A₁: [³H]-Chloro-N⁶-cyclopentyladenosine ([³H]CCPA)^[50]; A_{2A}: [³H]-3-(3-hydroxypropyl)-1-propargyl-7-methyl-8-(*m*-methoxystyryl)xanthine ([³H]MSX-2)^[34]; A_{2B}: [³H]-8-(4-(4-(4-chlorophenyl)piperazine-1-sulfonyl)phenyl)-1-propylxanthine ([³H]PSB-603)^[35]; A₃: [³H]-2-phenyl-8-ethyl-4-methyl-(8*R*)-4,5,7,8-tetrahydro-1*H*-imidazo[2,1-*f*]purine-5-one ([³H]PSB-11)^[36]. Initially, a single high concentration of compound was tested. For potent compounds, full concentration-inhibition curves were determined using different concentrations of test compounds spanning 3 orders of magnitude. At least three independent experiments were performed. Data were analyzed using the PRISM program version 4.0 or higher (Graph Pad, San Diego, CA, USA)

Monoamino oxidase assays

Screening: the inhibitors' activity was measured in the presence of substrate (*p*-tyramine 200 μM) and 1 μM of inhibitor (test compounds or reference compounds). The enzyme used for the experiments was human recombinant MAO-B from Sigma Aldrich. Results are presented as percentage of inhibition. Compounds that inhibited the enzyme by more than 50% of pargyline 10 μM (or rasagiline 1 μM, or safinamide 1 μM) activity are chosen for further tests (dose-response curves and IC₅₀ value).

Dose-dependent curves and IC₅₀: basing on the results from the screening, a range of dilutions for each compound was prepared and IC₅₀ values were determined and calculated.

ADMET estimation in vitro

Reference compounds

The compounds used as the references: caffeine (CFN), carbonyl cyanide 3-chlorophenyl-hydrazone (CCCP), doxorubicin (DX), ketoconazole (KE), sulfaphenazole (SE), quinidine (QD) were obtained from Sigma-Aldrich (St. Louis, MO, USA). Verapamil (VPL) was provided with the luminescent Pgp-Glo™ Assay System (Promega, Madison, WI, USA).

Affinity to glycoprotein-P

The test was performed with using commercial Pgp-Glo Assay System (Promega, Madison, WI, USA), according to the protocol provided by manufacturer. The reactions were prepared in triplicate in white polystyrene, flat-bottom Nunc™ MicroWell™ 96-well microplates (Thermo Scientific, Waltham, MA USA). The measurements of ATP-consuming by Pgp were done by microplate reader (EnSpire) in luminescence mode. Basal activity of Pgp was considered as the difference in the luminescent signal between samples treated with 100 μM of the selective Pgp inhibitor (sodium vanadate, 100% inhibition observed) and untreated samples. VPL with stimulatory activity on Pgp was used as reference

Influence on CYP activity

The study was performed using CYP3A4, CYP2D6 and CYP2C9 P450-Glo™ assays purchased from Promega (Madison, WI, USA). **13e** and **16a** were tested in triplicate at 10 μM. The study was performed with use of the proper reference inhibitors: KE, QD and SE

Metabolic stability

The metabolic stability was determined by human liver microsomes (HLMs) (Sigma-Aldrich, St. Louis, MO, USA) in 10 mM Tris-HCl buffer (pH

FULL PAPER

7.4). The *in vitro* evaluation of metabolic pathways was performed by 120 min incubation of **13e** and **16a** with HLMs at 37 °C in the presence of NADPH Regeneration System (Promega, Madison, WI, USA). UPLC/MS and MS ion fragment analyses were done by Waters ACQUITY TQD system with the TQ Detector (Waters, Milford, USA). The *in silico* prediction of metabolic biotransformations was performed by MetaSite 6.0.1 software (Molecular Discovery Ltd, Hertfordshire, UK).

Hepatotoxicity assays

Hepatotoxicity was estimated using hepatoma HepG2 (ATCC® HB-8065™) cell lines according to described previously protocols. The CellTiter 96® AQueous Non-Radioactive Cell Proliferation Assay was used from Promega (Madison, WI, USA). The compounds were investigated in quadruplicate at four concentrations (1, 10, 50 and 100 μM) for 72 h. The antiproliferative drug DX in dose 1 μM and mitochondrial toxin CCCP (10 μM) were used as a positive controls.

Molecular docking studies

A₁AR / A_{2A}AR

Recently described co-crystal structures of human adenosine A₁ (PDB ID: 5N2S) and A_{2A} (PDB ID: 3REY) receptors in complex with PSB36^[51] and XAC respectively were imported into MOE v. 2019.01 (ff used - AMBER10:EHT) and prepared using implemented QuikPrep tool: protonation states were generated using Protonate-3D tool, receptor tether strength – 5000, remove water molecules farther than 4.5 Å from ligand^[52]. Ligand library was prepared using Conformational Search tool using default settings. 5 lowest energy conformers were then docked to the rigid form of receptor, with site centred on ligand atoms using Wall Constraint (Placement method: Triangle Matcher, 30 poses to retain before refinement, 10 final poses scored GBVI/WSA dG scoring method). Possible binding pocket adaptation in presence of certain ligands was examined using Induced fit refinement protocol. In order to validate the methods used, co-crystallized ligands were redocked to crystal structures. The superposition of the phenylpurinedione cores with the co-crystallized ligands were of high confidence. Dynamics simulations (in time of 600 ps, T=300 K) were performed using the Nosé-Poincaré-Andersen equations of motion, forcefield AMBER10:EHT; R-Field 1:80, Cutoff (8,10).

MAO-A / MAO-B

For docking purposes, Schrödinger Maestro Suite^[53] was used. Ligands were built in their 3D forms and their bioactive conformations were generated using ConfGen module (water environment, target number of conformers – 20)^[54,55]. Crystal structures: 3REY and 2V5Z were prepared for docking using Protein Preparation Wizard^[56], ligand binding sites were centered on bound ligands. Docking to rigid form of receptor was performed using Glide module^[57] (precision standard, flexible ligand sampling, max 5 poses per conformer). The resulting structures were then submitted for energy minimization using procedure described in^[58]. Ligands were rated according their position in binding pocket, interactions with binding pocket amino acids as well as the docking score value. Possible binding pocket adaptation in presence of certain ligands was examined using Induced fit protocol (van der Waals radius radius scaling factor of 0.5, OPLS-2005 force field induced minimization, 10 output poses submitted to Prime with 5 Å cutoff)^[59].

Ligand interaction diagrams were generated using Schrödinger Maestro and MOE, ligand-receptor visualizations were generated using UCSF Chimera^[60]

Abbreviations

[³H]CCPA, [³H]2-Chloro-N⁶-cyclopentyladenosine; [³H]MSX-2, [³H]3-(3-hydroxypropyl)-1-propargyl-7-methyl-8-(*m*-methoxystyryl)xanthine;

[³H]PSB-11, [³H]2-phenyl-8-ethyl-4-methyl-(8*R*)-4,5,7,8-tetrahydro-1*H*-imidazo[2,1-*f*]purine-5-one; [³H]PSB603, [³H]8-(4-(4-(4-chlorophenyl)piperazine-1-sulfonyl)phenyl)-1-propylxanthine; AD, Alzheimer's disease; ADMET, absorption, distribution, metabolism, excretion, toxicity; AR, adenosine receptor; ASN, asparagine; ATP, adenosine triphosphate; cAMP, cyclic adenylylase monophosphate; CCCP, cyanide 3-chlorophenyl-hydrazone; CH₂Cl₂, dichloromethane; CHO, Chinese hamster ovary; CSC, 8-chlorostyrylcaffeine; DDI, drug-drug interactions; DIPEA, N,N-Diisopropylethylamine; DMF, Dimethylformamide; DMSO, dimethyl sulfoxide; FAD, flavin adenine dinucleotide ;ff, forcefield; GLN, glycine; GLU, glutamic acid; H₂O₂, hydrogen peroxide; HD, Huntington's disease; HLMs, human liver microsomes; IC₅₀, half maximal inhibitory concentration; ILE, isoleucine; K_i, inhibitory constant; LEU, leucine; MAO, monoaminoxidase; MeOH, methanol; MET, methionine; MTDL, multitarget directed ligand; ND, neurodegenerative diseases; PD, Parkinson's disease; PDB, Protein Data Bank; Pgp, P-glycoprotein; PHE, phenylalanine; RMSD, root mean square deviation; SAF, Safinamide; SER, serine; TM, transmembrane domain; TYR, tyrosine; WHO, world health organization; XAC, xanthine amine congener

Acknowledgements

Financial support by the Polish National Science Center grants based on decision No DEC-2016/23/N/NZ7/00475 and DEC-2018/02/X/NZ7/00584 as well as Jagiellonian University Medical College grants no. N42/DBS/000041 & N42/DBS/000039 are gratefully acknowledged.

Keywords: adenosine receptors, dual target ligands, monoamine oxidase B, molecular docking

References:

- [1] WHO, *World Report on Ageing and Health*, **2015**.
- [2] A. K. Kakkar, N. Dahiya, *Eur. J. Pharmacol.* **2015**, *750*, 74–81.
- [3] M. E. Freitas, S. H. Fox, *Neurodegener. Dis. Manag.* **2016**, *6*, 249–268.
- [4] T. J. Wenzel, A. Klegeris, *Life Sci.* **2018**, *207*, 314–322.
- [5] M. B. H. Youdim, L. Kupersmidt, T. Amit, O. Weinreb, *Parkinsonism Relat. Disord.* **2014**, *20*, S132–S136.
- [6] W. J. Geldenhuys, C. J. Van der Schyf, *Expert Opin. Drug Discov.* **2013**, *8*, 115–129.
- [7] L. Pisani, M. Catto, F. Leonetti, O. Nicolotti, A. Stefanachi, F. Campagna, A. Carotti, *Curr Med Chem* **2011**, *18*, 4568–4587.
- [8] A. Cavalli, M. L. Bolognesi, A. Minarini, M. Rosini, V. Tumiatti, M. Recanatini, C. Melchiorre, *J. Med. Chem.* **2008**, *51*, 347–372.
- [9] B. Mathew, D. G. T. Parambi, G. E. Mathew, M. S. Uddin, S. T. Inasu, H. Kim, A. Marathakam, M. K. Unnikrishnan, S.

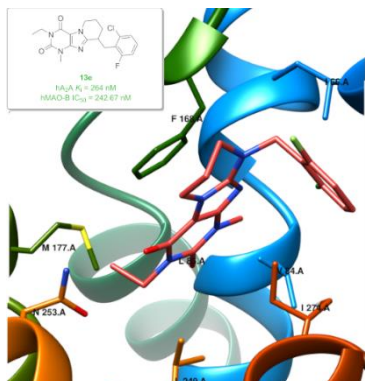
FULL PAPER

- Carradori, *Arch. Pharm. (Weinheim)*. **2019**, *352*, 1–13.
- [10] J. P. Petzer, N. Castagnoli, M. a Schwarzschild, J. Chen, *Neurotherapeutics* **2009**, *6*, 141–151.
- [11] A. Stößel, M. Schlenk, S. Hinz, P. Küppers, J. Heer, M. Gütschow, C. E. Müller, *J. Med. Chem.* **2013**, *56*, 4580–4596.
- [12] M. Jaiteh, A. Zeifman, M. Saarinen, P. Svenningsson, J. Bréa, M. Isabel Loza, J. Carlsson, *J. Med. Chem.* **2018**, *61*, 5269–5278.
- [13] S. Aoyama, H. Kase, E. Borrelli, *J. Neurosci.* **2000**, *20*, 5848–5852.
- [14] B. C. Shook, P. F. Jackson, *ACS Chem. Neurosci.* **2011**, *2*, 555–567.
- [15] G. Navarro, A. Cordoní, V. Casadó-Anguera, E. Moreno, N.-S. Cai, A. Cortés, E. I. Canela, C. W. Dessauer, V. Casadó, L. Pardo, et al., *Nat. Commun.* **2018**, *9*, 1242.
- [16] M. Rivera-Oliver, M. Díaz-Ríos, *Life Sci.* **2014**, *101*, 1–9.
- [17] C. Laurent, S. Eddarkaoui, M. Derisbourg, A. Leboucher, D. Demeyer, S. Carrier, M. Schneider, M. Hamdane, C. E. Müller, L. Buée, et al., *Neurobiol. Aging* **2014**, *35*, 2079–2090.
- [18] A. Pinna, N. Simola, L. Frau, M. Morelli, in *Adenosine*, Springer New York, New York, NY, **2013**, pp. 361–384.
- [19] P. Hickey, M. Stacy, *Curr. Neurol. Neurosci. Rep.* **2012**, *12*, 376–385.
- [20] F. F. Ribeiro, S. Xapelli, C. Miranda-Lourenço, S. R. Tanqueiro, J. Fonseca-Gomes, M. J. Diógenes, J. A. Ribeiro, A. M. Sebastião, *Neuropharmacology* **2016**, *104*, 226–242.
- [21] M. Kolahdouzan, M. J. Hamadeh, *CNS Neurosci. Ther.* **2017**, *23*, 272–290.
- [22] M. D. Mertens, S. Hinz, C. E. Müller, M. Gütschow, *Bioorganic Med. Chem.* **2014**, *22*, 1916–1928.
- [23] B. Strydom, J. J. Bergh, J. P. Petzer, *Eur. J. Med. Chem.* **2011**, *46*, 3474–3485.
- [24] M. B. H. Youdim, Y. S. Bakhle, *Br. J. Pharmacol.* **2009**, *147*, S287–S296.
- [25] J.-F. Chen, Y. Chem, Springer, Berlin, Heidelberg, **2011**, 267–310.
- [26] V. Flaten, C. Laurent, J. E. Coelho, U. Sandau, V. L. Batalha, S. Burnouf, M. Hamdane, S. Humez, D. Boison, L. V. Lopes, et al., *Biochem. Soc. Trans.* **2014**, *42*, 587–592.
- [27] R. Dungo, E. D. Deeks, *Drugs* **2013**, *73*, 875–882.
- [28] S. Rivara, G. Piersanti, F. Bartocchini, G. Diamantini, D. Pala, T. Riccioni, M. A. Stasi, W. Cabri, F. Borsini, M. Mor, et al., *J. Med. Chem.* **2013**, *56*, 1247–1261.
- [29] P. Koch, R. Akkari, A. Brunschweiler, T. Borrmann, M. Schlenk, P. Küppers, M. Köse, H. Radjainia, J. Hockemeyer, A. Drabczyńska, et al., *Bioorg. Med. Chem.* **2013**, *21*, 7435–7452.
- [30] M. Zaluski, J. Schabikowski, M. Schlenk, A. Olejarz-Maciej, B. Kubas, T. Karcz, K. Kuder, G. Latacz, M. Zygmunt, D. Synak, et al., *Bioorg. Med. Chem.* **2019**, *27*, 1195–1210.
- [31] M. Zaluski, K. Stanuch, T. Karcz, S. Hinz, G. Latacz, E. Szymańska, J. Schabikowski, A. Doróż-Płonka, J. Handzlik, A. Drabczyńska, et al., *MedChemComm* **2018**, *9*, 951–962.
- [32] A. Drabczyńska, M. Zygmunt, J. Sapa, B. Filipek, C. E. Müller, K. Kieć-Kononowicz, *Arch. Pharm. (Weinheim)*. **2011**, *344*, 20–27.
- [33] K.-N. Klotz, M. J. Lohse, U. Schwabe, G. Cristalli, S. Vittori, M. Grifantini, *Naunyn-Schmiedeberg Arch. Pharmacol.* **1989**, *340*, 679–683.
- [34] C. E. Müller, J. Maurinsh, R. Sauer, *Eur. J. Pharm. Sci.* **2000**, *10*, 259–265.
- [35] T. Borrmann, S. Hinz, D. C. G. Bertarelli, W. Li, N. C. Florin, A. B. Scheiff, C. E. Müller, *J. Med. Chem.* **2009**, *52*, 3994–4006.
- [36] C. E. Müller, M. Diekmann, M. Thorand, V. Ozola, *Bioorg. Med. Chem. Lett.* **2002**, *12*, 501–503.
- [37] G. Latacz, A. S. Hogendorf, A. Hogendorf, A. Lubelska, J. M. Wierońska, M. Woźniak, P. Cieślak, K. Kieć-Kononowicz, J. Handzlik, A. J. Bojarski, *MedChemComm* **2018**, *9*, 1882–1890.
- [38] G. Latacz, A. Lubelska, M. Jastrzębska-Więsek, A. Partyka, M. A. Marć, G. Satała, D. Wilczyńska, M. Kotańska, M. Więcek, K. Kamińska, et al., *Int. J. Mol. Sci.* **2019**, *20*, 3420.
- [39] G. Latacz, A. Lubelska, M. Jastrzębska-Więsek, A. Partyka, A. Sobilo, A. Olejarz, K. Kucwaj-Brysz, G. Satała, A. J. Bojarski, A. Wesołowska, et al., *Chem. Biol. Drug Des.* **2017**, *90*, 1295–1306.
- [40] G. Latacz, A. Lubelska, M. Jastrzębska-Więsek, A. Partyka, K. Kucwaj-Brysz, A. Wesołowska, K. Kieć-Kononowicz, J.

FULL PAPER

- Handzlik, *Bioorg. Med. Chem. Lett.* **2018**, *28*, 878–883.
- [41] L. Smetanova, V. Stetinova, D. Kholova, J. Kvetina, J. Smetana, Z. Svoboda, *Neuroendocrinol. Lett.* **2009**, *30*, 101–105.
- [42] R. K. Y. Cheng, E. Segala, N. Robertson, F. Deflorian, A. S. Doré, J. C. Errey, C. Fiez-Vandal, F. H. Marshall, R. M. Cooke, *Structure* **2017**, *25*, 1275-1285.e4.
- [43] S. Weyler, F. Fülle, M. Diekmann, B. Schumacher, S. Hinz, K.-N. Klotz, C. E. Müller, *ChemMedChem* **2006**, *1*, 891–902.
- [44] E. Szymańska, A. Drabczyńska, T. Karcz, C. E. Müller, M. Köse, J. Karolak-Wojciechowska, A. Fruziński, J. Schabikowski, A. Doroz-Plonka, J. Handzlik, et al., *Bioorg. Med. Chem.* **2016**, *24*, 4347–4362.
- [45] A. S. Doré, N. Robertson, J. C. Errey, I. Ng, K. Hollenstein, B. Tehan, E. Hurrell, K. Bennett, M. Congreve, F. Magnani, et al., *Structure* **2011**, *19*, 1283–1293.
- [46] C. Binda, J. Wang, L. Pisani, C. Caccia, A. Carotti, P. Salvati, D. E. Edmondson, A. Mattevi, *J. Med. Chem.* **2007**, *50*, 5848–52.
- [47] S.-Y. Son, J. Ma, Y. Kondou, M. Yoshimura, E. Yamashita, T. Tsukihara, *Proc. Natl. Acad. Sci. U. S. A.* **2008**, *105*, 5739–44.
- [48] P. Koch, R. Akkari, A. Brunschweiler, T. Borrmann, M. Schlenk, P. Küppers, M. Köse, H. Radjainia, J. Hockemeyer, A. Drabczyńska, et al., *Bioorg. Med. Chem.* **2013**, *21*, 7435–7452.
- [49] A. Brunschweiler, P. Koch, M. Schlenk, F. Pineda, P. Küppers, S. Hinz, M. Köse, S. Ullrich, J. Hockemeyer, M. Wiese, et al., *ChemMedChem* **2014**, *9*, n/a-n/a.
- [50] K. K. Martin, J. L. Ulrich, G. Cristalli, S. Vittori, M. Grifantini, **1989**, 679–683.
- [51] R. K. Y. Cheng, E. Segala, N. Robertson, F. Deflorian, A. S. Doré, J. C. Errey, C. Fiez-Vandal, F. H. Marshall, R. M. Cooke, *Structure* **2017**, *25*, 1275-1285.e4.
- [52] Molecular Operating Environment (MOE), 2019.01; <https://www.chemcomp.com/> (last accessed **12.12.2019**)
- [53] Schrödinger Release 2019-1: Schrödinger, LLC, New York, NY, **2016**.
- [54] K. S. Watts, P. Dalal, R. B. Murphy, W. Sherman, R. A. Friesner, J. C. Shelley, *J. Chem. Inf. Model.* **2010**, *50*, 534-546
- [55] Schrödinger Release 2019-1: ConfGen, Schrödinger, LLC, New York, NY (**2019**).
- [56] Schrödinger Release 2019-1: Protein Preparation Wizard; Schrödinger, LLC, New York, NY, **2019**
- [57] Schrödinger Release 2019-1: Glide, Schrödinger, LLC, New York, NY, **2019**
- [58] M. Gidaro, F. Alcaro, S. Carradori, G. Costa, D. Vullo, C. Supuran, S. Alcaro, *Planta Med.* **2015**, *81*, 533–540.
- [59] Schrödinger Release 2019-1: Induced Fit Docking protocol; Glide, Schrödinger, LLC, New York, **2019**; Prime, Schrödinger, LLC, New York, **2019**
- [60] E. F. Pettersen, T. D. Goddard, C. C. Huang, G. S. Couch, D. M. Greenblatt, E. C. Meng, T. E. Ferrin, *J. Comput. Chem.* **2004**, *25*, 1605–1612.

Entry for the Table of Contents



A series of 19 novel, *f*-bond annelated xanthine ligands with expected dual A_{2A}AR/MAO-B inhibitory activity was obtained. The lead compound that might act as dual ligand, appeared to be **13e** (A_{2A}AR K_i =264 nM, MAO-B IC_{50} =243 nM) and has therefore potential for the treatment of PD and AD with expected symptomatic and neuroprotective effects. However, further structural modifications of **13e** in order to improve its ADMET properties are required.